

- ***ADVANCED HOT GAS FILTER  
DEVELOPMENT***

*for Period September 29, 1994 - September 30, 1998  
for DE-AC21-94MC31212 -01*

- ***Prepared for:***

*U. S. Department of Energy  
Office of Fossil Energy  
Federal Energy Technology Center  
Morgantown, WV 26507*

- ***Prepared by:***

*McDERMOTT TECHNOLOGY INC.  
a McDermott company*

*P. O. Box 11165  
Lynchburg, VA 24506*

McDermott Technology, Inc. Assumes no liability with respect to the use of, or for damages resulting from the use of, or makes any warranty or representation regarding any information, apparatus, method, or process disclosed in this report.

McDermott Technology, Inc. expressly excludes any and all warranties either expressed or implied, which might arise under law or custom or trade, including without limitation, warranties of merchantability and of fitness for specified or intended purpose.

# TABLE OF CONTENTS

<u>SECTION</u>	<u>PAGE</u>
<b>EXECUTIVE SUMMARY</b> .....	2
<b>1.0 INTRODUCTION</b> .....	4
<b>2.0 BACKGROUND INFORMATION</b> .....	5
<b>3.0 PROGRAM OBJECTIVES</b> .....	7
<b>4.0 FABRICATION APPROACH</b> .....	8
4.1 RAW MATERIALS .....	8
4.1.1 Continuous Fiber .....	8
4.1.1.1 Fiber Coating .....	10
4.1.2 Chopped Fiber .....	10
4.1.3 Binders .....	10
4.1.3.1 Phosphoric Acid .....	10
4.1.3.2 Boehmire .....	11
4.1.3.3 Thermal Bonded .....	11
4.2 VACUUM WINDING PROCESS .....	11
4.3 BONDING .....	12
4.4 HEAT TREATING .....	13
4.5 TEST METHODS .....	13
4.5.1 Permeability .....	13
4.5.2 C-ring Strength .....	13
4.5.3 Microstructure .....	14
<b>5.0 OPEN-END TUBE FABRICATION AND TESTING</b> .....	15
5.1 VACUUM WINDING .....	15
5.2 PERMEABILITY .....	15
5.3 C-RING STRENGTH .....	15
5.4 CONCLUSION AND RECOMMENDATIONS .....	16
<b>6.0 SUB-SCALE ELEMENTS</b> .....	17
6.1 FILAMENT WINDING .....	17
6.2 COAL COMBUSTION EXPOSURE TEST .....	17
6.3 RESULTS AND DISCUSSION .....	19
6.3.1 Permeability .....	19
6.3.2 C-ring Strength .....	19
6.3.3 Microstructure .....	20
6.4 CONCLUSION AND RECOMMENDATIONS FOR FULL-SCALE ELEMENTS .....	22

## TABLE OF CONTENTS, CONTINUED

**SECTION**  
**PAGE**

<b>7.0</b>	<b>FULL-SCALE FILTER ELEMENTS: ONE METER ELEMENTS</b> .....	23
7.1	VACUUM WINDING .....	23
7.2	BONDING .....	23
7.3	FLANGE MACHINING ISSUES .....	23
7.4	W-STC HTHP TEST .....	24
	7.4.1 Filter Issues .....	24
7.5	RESULTS AND DISCUSSION .....	24
	7.5.1 Composition .....	24
	7.5.2 Permeability .....	24
	7.5.3 C-ring Strength .....	25
	7.5.4 Microstructure .....	25
7.6	CONCLUSIONS AND RECOMMENDATIONS .....	26
<b>8.0</b>	<b>FILTER IMPROVEMENT AND COST REDUCTION</b> .....	27
8.1	VACUUM WINDING .....	27
	8.1.1 Nextel Fiber Shape .....	27
	8.1.2 Fiber Architecture .....	27
	8.1.3 Net Shape Flange .....	28
8.2	BONDING .....	28
8.3	RESULTS AND DISCUSSION .....	29
	8.3.1 C-ring Strength and Permeability .....	29
8.4	CONCLUSIONS AND RECOMMENDATIONS .....	29
<b>9.0</b>	<b>FABRICATION OF 50 ELEMENTS FOR TESTING: KARHULA PCFB TEST</b> .....	30
9.1	RESULTS AND DISCUSSION .....	30
	9.1.1 Composition and Permeability .....	30
	9.1.2 Surface Defects .....	30
	9.1.3 C-ring Strength .....	31
9.2	CONCLUSIONS AND RECOMMENDATIONS .....	31
<b>10.0</b>	<b>FABRICATION OF 50 ELEMENTS FOR TESTING: PSDF TEST</b> .....	32
10.1	RESISTS AND DOSSISOPM .....	32
	10.1.1 Composition and Permeability .....	32
	10.1.2 PSDF TC02 Thermal Excursion .....	32
<b>11.0</b>	<b>CFCC MODELING AND TESTING SUPPORT</b> .....	33

**TABLE OF CONTENTS, CONTINUED**

<b><u>SECTION</u></b>	<b><u>PAGE</u></b>
<b>12.0 CONCLUSIONS AND RECOMMENDATIONS .....</b>	<b>34</b>
12.1 BENEFITS OF THE MTI VACUUM WOUND FILTER ELEMENT .....	34
12.2 DEVELOPMENT STATUS AND MANUFACTURING SCALE-UP .....	34
12.3 FUTURE WORK .....	35
<b>APPENDIX A: NEXTEL CERAMIC FIBER PROPERTIES .....</b>	<b>84</b>
<b>APPENDIX B: SAFFIL PROPERTIES .....</b>	<b>85</b>
<b>APPENDIX C: NYACOL COLLOIDAL ALUMINA PROPERTIES .....</b>	<b>89</b>
<b>REFERENCES .....</b>	<b>90</b>

**TABLES**

<b><u>NUMBER</u></b>		<b><u>PAGE</u></b>
1	Open-end tube compositions .....	36
2	Open-end tube properties .....	36
3	Sub-scale candidate filter compositions .....	37
4	Properties of sub-scale hot gas filter elements .....	37
5	Filter element composition and fiber architecture for W-STC test in 8/96.	38
6	TS2-97 Test campaign at the Foster Wheeler pressurized circulating fluid bed combustion test facility in Karhula, Finland .....	38
7	PSDF run summary .....	39
8	Field exposure test summary .....	39
9	MTI hot gas filter status .....	39

**FIGURES**

<b><u>NUMBER</u></b>		<b><u>PAGE</u></b>
1	Vacuum winding schematic.....	40
2	Composition C1 open-end tube compressive C-ring results .....	41
3	Composition C2 open-end tube compressive C-ring results .....	42
4	Composition C3 open-end tube compressive C-ring results .....	43
5	Ebensburg Power/B&W 55 Mwe circulating fluid bed combustion unit ....	44
6	Sample probe for sub-scale samples and observation port .....	45
7	As-fabricated compressive C-ring results for sub-scale elements .....	46

**TABLE OF CONTENTS, CONTINUED**

## FIGURES

<u>NUMBER</u>		<u>PAGE</u>
8	Compressive C-ring results for CFB (816C) samples .....	47
9	Compressive C-ring results for CFB (885C) samples .....	48
10	Compressive C-ring results for CFB fatigue samples .....	49
11	Summary compressive C-ring results for composition C3 .....	50
12	20X BSE of sample C1-4 .....	51
13	A. 500X BSE image of fiber tow bundle in sample C1-4 from CFB thermal fatigue test.	
	B. 2000X BSE image of individual Almax fibers and bond phase from sample C1-4 .....	52
14	A. 500X BSE image of chopped fiber region of sample C1-4 from CFB thermal fatigue test	
	B. 2000X BSE of boehmite bonded chopped fiber from sample C1-4 .....	53
15	20X BSE image of sample C2-2 from thermal fatigue exposure test .....	54
16	A. 500X BSE image of Nextel 610 fiber tow in sample C2-2 from CFB thermal fatigue test	
	B. 2000X BSE image of Nextel 610 fibers and bond phase from sample C2-2 .....	55
17	A. 500X BSE image of chopped fiber region of sample C2-2 from CFB thermal fatigue test	
	B. 2000X BSE image of chopped fibers and bond phase in sample C2-2 ..	56
18	20X BSE image of sample C3-2 from CFB thermal fatigue test .....	57
19	A. 500X BSE image of Nextel 610 fiber tow from sample C3-2 following CFB thermal fatigue test .....	58
20	A. 500X BSE image of chopped fiber region of sample C3-2 following CFB thermal fatigue test	
	B. 2000X BSE image of chopped fiber and bond phase from sample C3-2 .....	59
21	20X BSE image of sample C4-4 from CFB thermal fatigue test .....	60
22	A. 500X BSE image of Nextel 610 fiber tow from sample C4-4	
	B. 2000X BSE image of individual Nextel 610 fibers in sample C4-4 .....	61
23	A. 500X BSE image of boehmite bonded chopped fibers in sample C4-4 from CFB thermal fatigue test	
	B. 2000X BSE image of boehmite bonded chopped fiber in sample C4-4 .....	62
24	Machined flange configuration .....	63
25	Flange test configuration and load-displacement results .....	64
26	Composition and pressure drop results for W-STC HTHP 8/96 test .....	65
27	Compressive C-ring results for as-fabricated and post-test HTHP 8/96 test elements .....	66

### TABLE OF CONTENTS, CONTINUED

## FIGURES

<b><u>NUMBER</u></b>		<b><u>PAGE</u></b>
28	20X BSE image of as-fabricated sample 6-6-10 .....	67
29	150X BSE image of chopped fiber region in sample 6-6-10.....	68
30	10X BSE image of sample 6-6-19 after W-STC HTHP test .....	69
31	150X BSE image of as-fabricated sample 6-6-19 after W-STC HTHP test .....	70
32	20X BSE image of the OD surface of sample 6-6-17 after W-STC HTHP test .....	71
33	1000X BSE image of the OD surface of sample 6-6-17 after W-STC HTHP test .....	72
34	150X BSE image of sample 6-6-6 after W-STC HTHP test .....	73
35	5X macrophoto of unserved Nextel 610 fiber .....	74
36	5X Macrophoto of rayon served Nextel 610 fiber.....	75
37	Example of controlled fiber distribution .....	76
38	Net shape flange configuration .....	77
39	Compressive C-ring results for controlled fiber distribution with boehmite bond .....	78
40	Fiber element composition and permeabilities for Karhula PCFB test .....	79
41	Surface defect on Karhula element .....	80
42	As-fabricated and post-test load-displacement results for Karhula elements .....	81
43	Composition and permeability of PSDF element.....	82
44	Flange bend test configuration and load versus displacement results.....	83

## ACKNOWLEDGMENTS

The assistance of T. J. McMahon, FETC COR, is gratefully acknowledged. In addition, the U.S. Department of Energy Continuous Ceramic Fiber Composite program has provided valuable material development support for this project. Finally, the hot gas filter modeling and testing performed at Virginia Tech by Dr. K. Reifsnider and his students X. Huang and R. Carter under the CFCC program and the Virginia's Center for Innovative Technology provided valuable understanding of the structural response of the vacuum wound material.

**Project Title:** Advanced Hot Gas Filter Development

**Reporting Period:** September 29, 1994 - September 30, 1998

**Principal Author:** Richard A. Wagner

**Approved By:** Eric A. Barringer, Manager, Advanced Materials Section

**Date Report was Issued:** November 18, 1998

**Award Number:** DE-AC21-94MC31212

**For:** U. S. Department of Energy  
Office of Fossil Energy  
Federal Energy Technology Center  
Morgantown, WV

**By:** McDermott Technology Inc  
PO Box 11165  
Lynchburg, VA 24506-1165

## **EXECUTIVE SUMMARY**

This report describes the fabrication and testing of continuous fiber ceramic composite (CFCC) based hot gas filters. The fabrication approach utilized a modified filament winding method that combined both continuous and chopped fibers into a novel microstructure. The work was divided into five primary tasks. In the first task, a preliminary set of compositions was fabricated in the form of open end tubes and characterized. The results of this task were used to identify the most promising compositions for sub-scale filter element fabrication and testing. In addition to laboratory measurements of permeability and strength, exposure testing in a coal combustion environment was performed to assess the thermo-chemical stability of the CFCC materials. Four candidate compositions were fabricated into sub-scale filter elements with integral flange and a closed end. Following the 250 hour exposure test in a circulating fluid bed combustor, the retained strength ranged from 70 to 145 percent of the as-fabricated strength. The post-test samples exhibited non-catastrophic failure behavior in contrast to the brittle failure exhibited by monolithic materials.

Filter fabrication development continued in a filter improvement and cost reduction task that resulted in an improved fiber architecture, the production of a net shape flange, and an improved low cost bond. These modifications were incorporated into the process and used to fabricate 50 full-sized filter elements for testing in demonstration facilities in Karhula, Finland and at the Power Systems Development Facility (PSDF) in Wilsonville, AL. After 581 hours of testing in the Karhula facility, the elements retained approximately 87 percent of their as-fabricated strength. In addition, mechanical response testing at Virginia Tech provided a further demonstration of the high level of strain tolerance of the vacuum wound filter elements. Additional testing in the M. W. Kellogg unit at the PSDF has accumulated over 1800 hours of coal firing at temperatures of 760 °C including a severe thermal upset that resulted in the failure of several monolithic oxide elements. No failures of any kind have been reported for the MTI CFCC elements in either of these test campaigns. Additional testing is planned at the M. W. Kellogg unit and Foster Wheeler unit at the PSDF over the next year in order to qualify for consideration for the Lakeland PCFB.

Process scale-up issues have been identified and manufacturing plans are being evaluated to meet the needs of future demand.

## **1.0 INTRODUCTION**

This report describes the fabrication and testing of continuous fiber ceramic composites (CFCC) based hot gas filters. The work was divided into three primary tasks. In the first task, a preliminary set of compositions was fabricated in the form of open-end tubes and characterized. The results of the first task were then used to identify the most promising compositions for sub-scale filter element fabrication and testing. In addition to laboratory measurements of permeability and strength, exposure testing in a coal combustion environment was performed in the second task to assess the thermo-chemical stability and thermal fatigue resistance of the CFCC materials. The results of this testing were then used to down-select the filter composition for full-scale filter fabrication and testing in the final phase of the program.

## **2.0 BACKGROUND INFORMATION**

Pressurized fluid bed combustion (PFBC) and integrated gasification combined cycle (IGCC) systems are among the advanced coal-based energy cycles being considered for low cost, clean power generation. A critical feature of these advanced coal fired power generation systems is the high temperature high-pressure gas stream utilized by the gas turbine. In order to protect the gas turbine components from erosion, it is necessary to remove the ash/sorbent particulates from the turbine inlet gas stream. In first generation PFBC plants such as Tidd, hot cyclones provided a sufficiently clean gas stream for the ruggedized turbine. Second generation combined cycle plants utilize a topping combustor and high temperature gas turbines that require barrier filters to meet the turbine inlet requirements. The high temperature barrier filters are therefore considered to be one of the enabling technologies for these high efficiency cycles. Testing at various DOE and private facilities has demonstrated that the level of mechanical durability exhibited by the currently available filters may not be adequate to meet the reliability demands of large power generation systems. Candle filters utilized in these systems consist of closed end ceramic tubes measuring 60 mm diameter by 1.5 meters long with a flanged open end. The wall thickness varies with the supplier and material used in the construction.

Hot gas filter elements must be sufficiently rugged to withstand the mechanical abuse associated with a power plant environment. Element failures have occurred during shipping, installation, and inspection/removal. Although failures during shipping or installation would not result in plant downtime, filter elements may be damaged to the extent that even normal operating conditions could lead to failure. During normal operations, the filter elements are exposed to temperatures up to 850 °C in a combustion atmosphere containing alkali, sulfur, and water vapor. As in many material applications, the nominal operating conditions of 750 to 860 °C in a coal combustion atmosphere present only part of the challenge. Plant upset conditions, on the other hand, typically present a serious threat to the filter element and account for the bulk of the failures. In some pilot scale screening tests, the thermal fatigue associated with accelerated back pulsing and the more severe thermal transients relating to turbine trips and combustor trips are simulated. Additional tests would be needed to simulate the more severe upsets associated with load changes or start up. For example, transition from startup burners to

coal firing may result in the carryover of unburned coal to the filter system and subsequent ignition on the surface of the filter element. Recent filter element failures were attributed to this type of operational upset that produced localized thermal gradients and associated stresses. In monolithic materials, the combination of a high elastic modulus and high coefficient of thermal expansion often results in excessive thermal stresses that produce catastrophic failure of the filter element.

Monolithic silicon carbide (SiC) is currently the most common material used in the fabrication of candle filters. Assuming a 40 mm inside diameter and 40% porosity, 1.5 meter long SiC elements weigh approximately 5 kg. Because of their monolithic structure, SiC candle filter elements exhibit brittle or catastrophic failure. The combination of relatively high thermal conductivity and moderate thermal expansion ( $5 \text{ ppm}/^{\circ}\text{C}$ ) of SiC contributes to good thermal shock resistance. Excessive creep elongation and distortion of SiC candle filter elements was attributed to the clay based bond phase used in some compositions. New bond systems have eliminated the creep problem; however, element elongation due to oxidation remains an issue at higher temperatures.

Mullite and cordierite oxide materials have also been utilized for monolithic ceramic barrier filters. Mullite systems suffer from low thermal shock resistance as a result of a moderate thermal conductivity and moderate thermal expansion ( $5 \text{ ppm}/^{\circ}\text{C}$ ). The low thermal expansion ( $1 \text{ to } 1.5 \text{ ppm}/^{\circ}\text{C}$ ) of cordierite systems results in increased thermal shock resistance; however, brittle failures remain a problem.

### **3.0 PROGRAM OBJECTIVES**

The objectives of this program are to develop toughened ceramic hot gas filters and evaluate these filters for application in Pressurized Fluidized Bed Combustor (PFBC) and Integrated Gasification Combined Cycle (IGCC) power generation systems. The essential requirements of a composite material designed to meet the program objective for a toughened hot gas filter include the following:

- stable continuous fiber
- rigid porous matrix
- engineered fiber-matrix interface
- appropriate permeability and filtration characteristics
- cost effectiveness

The development approach used to achieve these objectives started with 30 cm long open end tubes; progressed to flanged closed end sub-scale elements; and finally scaled the process up to the fabrication and testing of full size filter elements. Two McDermott operating divisions played key roles in the development and commercialization of an advanced hot gas filter. The BWXT division's expertise in filament winding was utilized in the development program and will also be the ultimate manufacturing facility for commercial filter element production. Babcock & Wilcox's Power Generation Group (PGG) experience in the design of advanced power systems including hot gas filter systems provided valuable guidance to this program. In addition, valuable material development activities supporting this work were performed under the DOE Continuous Fiber Ceramic Composite (CFCC) program.

## **4.0 FABRICATION APPROACH**

### **4.1 Raw Materials**

An all oxide composite material system was selected because it would be thermodynamically stable in the oxidizing atmosphere of a PFBC. The silica content was minimized to improve the alkali resistance.

#### 4.1.1 Continuous Fiber

Two pure alumina fibers, Mitsui's Almax and 3M's Nextel 610 were used as the continuous fiber reinforcements in the candidate composites. The Almax fiber consists of 1000 filament tows of polycrystalline fibers. The Nextel 610 fibers are comprised of 400 filament tows. The unit weights of the fibers are 2250 denier and 1500 denier for the Almax and Nextel 610 respectively.

#### 4.1.1 Fiber Coating

Fiber coatings are generally required to control the fiber/matrix interface in ceramic composite materials. A second consideration is the need to protect the continuous fibers from degradation during processing or in service. While the fiber architecture used in this work does not actually have a continuous matrix phase it is important that the bond system does not degrade the continuous fibers. Fugitive carbon coatings have been shown to be effective means of protecting the fibers in many composite systems. The fact that the carbon coating disappears in service is expected to have less of an affect on the long-term properties of an oxide composite system than for non-oxide systems. The silica reaction phase formed on non-oxide fibers in oxidizing environments will likely produce a strong bond between the fiber and matrix and result in more brittle fracture behavior. The primary function of the fiber coating in the MTI approach is to protect the reinforcement fibers from corrosive bonding solutions.

Candidate carbon precursors evaluated in this program included polyurethane resin, furfuryl alcohol, and pyrolyzed fiber sizing. Initial trials with an on-line polyurethane resin coating failed to provide adequate protection because it was used without drying or pyrolysis. Catalyzed furfuryl alcohol was also used in an on-line coating system that utilized a low temperature heat treatment to cross-link and stabilize the coating. The resultant fiber tows were considerably stiffer than the as received fiber tows and this resulted in very low preform densities. In addition, the slow speed of the on-line coating process interfered with the filament winding process and resulted in non-uniform distribution of the chopped fiber. The above considerations led to the selection of the pyrolyzed fiber sizings as the coating for the initial winding development. As-received fibers were re-spooled on to 3 inch diameter mullite tubes and pyrolyzed in to 870 °C in nitrogen. The Almax fibers are sized with a 5 wt. percent epoxy resin which yielded a relatively thick coating with considerable bridging between the filaments. The Nextel 610 170 resin sizing consists of 0.6 to 2.4 wt. percent ethoxylated polyethyleneimine and 0.2 to 1.2 wt. percent polyethyleneglycol and yielded a much thinner fiber coating when pyrolyzed to 870 °C in nitrogen.

An improved fiber coating process based on the work of Hay<sup>1</sup> was implemented under the CFCC Program for the sub-scale filter element fabrication task. This process utilized the differences in the interfacial energies of immiscible liquids to minimize the coating bridges that normally occur within the fiber tow. Furfuryl alcohol catalyzed with citric acid was used as the carbon precursor. Hexadecane is immiscible with the furfuryl alcohol and provided the difference in interfacial energy required to minimize bridging within the fiber tow bundle. The as-received Nextel 610 fiber was de-sized by heating to approximately 815 °C in air. The fiber tow then entered the catalyzed furfuryl alcohol solution and then continued up through the hexadecane to separate the filaments. An argon purged furnace operated at about 815 °C was used to first cross-link and then pyrolyze the fiber coating. Up to six coating passes were performed on each fiber tow before applying a PVA sizing to improve handling strength.

No coating was used in the alumina bond system because the Nyacol sol did not react with or degrade the continuous fibers.

#### 4.1.2 Chopped Fiber

The ICI Saffil discontinuous fiber (95-97% alumina, 3-5% silica) was supplied as bulk fiber and exhibited a mean diameter of 3.5 microns. Details of the properties of the various grades of Saffil fiber are given in Appendix A.

#### 4.1.3 Binders

Various binders were evaluated to develop bonding at the fiber to fiber contact points while maintaining acceptable permeability. Phosphoric acid and a boehmite sol were the primary binder systems in this work.

##### 4.1.3.1 Phosphoric Acid

Phosphoric acid was utilized as a bond system in the refractory industry for many years and details of the bonding reactions are given in the literature<sup>2</sup>. The use of phosphoric acid as a binder for metal matrix composite fiber preforms has also been reported<sup>3</sup>. Phosphoric acid reacts with the alumina fiber to form an aluminum metaphosphate gel on the fiber surface then converts to the final bonding phase,  $\text{AlPO}_4$ , on heating. Bonding occurred at the fiber to fiber contact points with minimal filling of the porosity of the fiber preform. Because phosphoric acid reacts with any source of alumina, the continuous fiber in the preform must be coated with an inert material such as carbon to minimize the reaction and the associated strength degradation. In addition, all heat treatments of the phosphoric acid bonded filter elements must be conducted in an inert atmosphere to preserve the carbon coating because the continuous fibers are vulnerable to the phosphate decomposition products. The use of uncoated continuous fibers with the phosphoric acid bond system resulted in brittle failures with little or no advantage over monolithic filter element systems.

#### 4.1.3.2 Boehmite

An oxyhydroxide of aluminum, AlOOH or boehmite was included as an alternative to the phosphoric acid bond system. According to McKenzie<sup>4</sup>, the boehmite transformations follow the sequence:



The initial transformation from the oxyhydroxide to alumina occurs between 450 and 580 °C depending on the crystallinity of the starting material. The final transition to  $\alpha$  alumina occurs at about 1200 °C. Single filament tests performed under the CFCC program demonstrated that the boehmite sol does not react with the Nextel fiber, thus no fiber coating is required.

#### 4.1.3.3 Thermal Bonded

Thermal bonding was considered as an alternative to the chemical or sol based binders described above. This concept was developed for the space shuttle thermal protection system tiles. A borosilicate bond system was used in various shuttle tile compositions<sup>5 6</sup>. A cordierite composition glass powder was selected and added to the Saffil slurry.

## 4.2 Vacuum Winding Process

McDermott Technology Inc. developed a unique filament winding process that uses both continuous and discontinuous oxide fibers to form a porous structure. The porous structure was then rigidized with a sol-gel based binder system and heat treated to complete the fabrication process. The resulting structure is essentially a fiber reinforced bulk filter that requires no filtration membrane and exhibits a high level of structural toughness and durability.

The objective of this task was to continue the development of the filament winding technology that was originally developed under the DOE sponsored CFCC Program (Contract

No. DE-FC02-92CE40945). The initial work focused on the production of 12 inch long open end filter samples with the desired dimensions (diameter and wall thickness). Particular attention was given to the development of a consistent macro/micro-structure over the length of the test specimen in terms of the relative amounts and distributions of the chopped and continuous fiber. Controlling this distribution is considered to be essential to achieving the desired properties. Four candidate compositions were included in this task. These compositions, given in Table 1, include variations in the type and amount of continuous fiber as well as an alternate bond system. The compositions were evaluated in terms of permeability, strength and fracture properties. The characterization results were then used to refine the test compositions used in the sub-scale fabrication task. Sub-scale tests provided guidance for full-scale filter development.

The general configuration of the vacuum winding process is shown in Figure 1. A Sahn fiber tensioner was used to control the tension of the continuous fiber. The Saffil fiber slurry was pumped onto the mandrel as the continuous fiber was filament wound. Initial windings were performed on a Cobra 2 axis filament winder. Subsequent test samples were produced on the computer controlled En-tec 4 axis filament winder. The four axes on the En-tec winder consisted of the spindle, horizontal carriage, rotating delivery eye, and vertical translation of the carriage. The chain driven Cobra winder required a unique set of drive sprockets and chain lengths for each set of winding parameters. In contrast, the programmable En-tec winder greatly facilitated changes in a wide variety of winding parameters such as sample diameter and length, fiber bandwidth, and fiber winding angle. Initial windings were performed using helical patterns and a 45° winding angle that resulted in a node length of approximately 150 mm. It is important to consider the fiber architecture when preparing test specimens that evaluate fiber-dominated properties such as C-rings or burst tests. For the 49 mm diameter mandrel used in this program, approximately 10 layers were required to achieve the 60 mm OD. The exact number of layers depended on the relative amount of continuous and chopped fiber.

### **4.3 Bonding**

The fabrication process was completed by the addition of a bond component in the form of a sol or liquid chemical binder to the filter element preform followed by heat treatments to convert the sol/chemical binder to a stable bond phase. The preform was first saturated with the

liquid binder and excess binder was removed under vacuum. An ideal bond system must develop bonds at fiber to fiber contact points without plugging or filling the open or continuous porosity of the filter element. The development of a uniform distribution of the bond phase is critical to developing high strength without compromising the permeability of the filter.

#### **4.4 Heat Treating**

An initial heat treatment to 538 °C was used to rigidize the sample sufficiently to remove it from the mandrel. A final heat treatment at 900 to 1150 °C was used to stabilize the bond. An inert atmosphere was used with the phosphoric acid bond system to preserve the carbon coating. Boehmite bonded samples were heat treated in air.

#### **4.5 Test Methods**

##### **4.5.1 Permeability**

The permeability of test specimens was determined at ambient conditions from the face velocity and the associated pressure drop across the specimen. The permeability equipment consists of a sample fixture, calibrated flow meter and a calibrated differential manometer. The face velocity is calculated by dividing the sample surface area by the volume flow rate.

##### **4.5.2 C-ring Strength**

Compressive C-ring tests were performed on a computer controlled mechanical test machine using calibrated load and deflection sensors. These tests were performed at room temperature and 871 °C. C-ring specimens were cut from the sample tubes using a diamond saw mounted on a lathe. A 25 mm wide specimen was considered to be the largest practical C-ring width even though winding pattern node length was about 150 mm. The maximum stress due to the applied load was calculated from the following expression:

$$S = \frac{P}{w \times t} \times \frac{R}{r_o} \times \frac{(r_o - r_i)}{r_o(r_o - R)}$$

P = peak load  
 w = ring width  
 t = wall thickness  
 r<sub>o</sub> = outer radius  
 r<sub>i</sub> = inner radius

$$R = \frac{r_o - r_i}{\ln(r_o/r_i)}$$

#### 4.5.3 Microstructure

The distribution and relative amounts of continuous fiber, chopped fiber, and bond phase was determined by examination of polished sections in an Etec scanning electron microscope (SEM) equipped with energy dispersive spectroscopy (EDS). The samples were vacuum impregnated with low viscosity resin in order to minimize open porosity in the mount. The resulting polished sections were difficult to interpret because of the high porosity of the material. Since it is not possible to fracture the samples into two pieces to obtain a fracture surface, an alternative sample preparation method was used to obtain a better indication of the open sample structure. Samples were vacuum impregnated with a thermal plastic (Aremco 509) and polished. The thermal plastic was dissolved in a solvent and then heated in air to 538 °C remove the residual resin. The resulting sample provided an unaltered structure for SEM examination.

## **5.0 OPEN-END TUBE FABRICATION AND TESTING**

### **5.1 Vacuum Winding**

Open-end tubes were fabricated by vacuum winding. The compositions and fiber architecture of the open-end tubes are given in Table 1. No usable preforms could be produced using Composition C4 because the powdered glass frit used sealed the preform during the initial winding closure and prevented subsequent deposition of chopped fiber.

### **5.2 Permeability**

The sample permeability results in Table 2 are reported as the pressure drop in inches of water at a face velocity of 10 ft/min. All of the tested compositions were at or below the allowable pressure drop of 10 inches of water.

### **5.3 C-ring Strength**

A summary of the C-ring test results for the open-end tubes is given in Table 2. Examples of the room temperature and elevated temperature fracture behavior of compositions C1, C2, and C3 are shown in Figures 2, 3, and 4, respectively. These results are plotted as stress versus percent strain. Figure 2 also includes the room temperature fracture behavior of a monolithic cordierite filter material. The observed brittle fracture is typical of monolithic ceramic materials. In comparison to the monolithic material, compositions C1 and C2 exhibited significantly greater strain to failure behavior at room temperature. The actual failure is probably a combined shear and tensile failure. Visual examination of the failed samples revealed that the primary failure ran through the channels of chopped fiber that occur between the continuous fiber tows. In addition, delaminations were evident which indicates that there was a significant shear component to the failure. At 871 °C, the fractures tended to be more brittle. The trend to more brittle high temperature failure is more obvious in the composition C2 shown in Figure 3. Similar results were reported<sup>7</sup> for dense composites using this bond system and it was attributed to matrix clamping of the continuous fiber as a result of mismatched thermal expansion between the fiber

and matrix. This explanation seems unlikely given the open fiber architecture of the current samples. The more brittle fracture behavior of composition C3 at both room temperature and high temperature, shown in Figure 4, is attributed to the lack of a coating on the continuous fibers. During the bonding operation, the continuous fibers were attacked by the bonding chemicals which degraded the fiber properties. This composition was included in the test matrix because the lack of a coating simplified the processing.

#### **5.4 Conclusion and Recommendations for Sub-scale Elements**

Based on the fabrication and testing results obtained on the open-end tubes, the following modifications were recommended for the sub-scale element fabrication task. Because of the fabrication problems encountered with composition C4, an alternate bond system was required to replace the glass-ceramic bond originally specified for composition C4. Therefore, the composition matrix was modified to include a boehmite bond system for compositions C1 and C4. Since the boehmite sol does not attack the continuous fibers, these compositions will not require a carbon coating. Furthermore, the high temperature failure behavior demonstrated that the coating produced by pyrolyzing the sizing provided inadequate protection of the continuous fibers in compositions C1 and C2. As discussed above, an immiscible liquid based fiber coating system was implemented to provide coated fibers for these compositions. Finally, in composition C3, carbon coated Nextel 610 fiber was substituted for the uncoated Almax fiber to minimize fiber degradation. This composition should result in the most uniform distribution of continuous fiber because of the smaller Nextel tow (400 filaments versus 1000 filaments for the Almax) The new compositions given in Table 3 were used to fabricate the sub-scale tubes.

## **6.0 SUB-SCALE ELEMENTS**

The filament winding procedure was modified to produce a prototypical flange and closed end on a 30 cm long sub-scale filter element.

### **6.1 Filament Winding**

Samples were prepared on the En-tec 4-axis winder using both helical and closed end winding programs. The mandrel was modified to include a spherical nose to form the closed end on the tube. For the 30 cm long sub-scale samples used in this program, the combination of the closed-end winding program and the 4<sup>th</sup> winder axis produced no practical advantage in terms of fiber distribution around the closed end. Furthermore, the winding rate decreased considerably as the fiber delivery head rotated and translated vertically to follow the profile of the closed end. This resulted in a very noticeable non-uniform distribution of chopped fiber that extended from the tube end to the first inch or more of the body. The helical winding pattern was therefore used for all sub-scale samples. The flange section was fabricated by alternating short hoop winding sections with the full-length helical winding. The programmable En-tec winder can link various programs to automatically include the hoop sections needed to build the required flange thickness. This fiber architecture resulted in a well anchored flange and is expected to minimize the potential for delamination.

### **6.2 Coal Combustion Exposure Test**

The objective of the exposure test was to establish the chemical durability of the sub-scale filter in a coal combustion environment. The original plan was to perform the coal combustion test in the Tidd PFBC, or in the event that the Tidd unit had shut down, the test would be performed in the small boiler simulator (SBS) at the MTI Alliance Research Center. The SBS utilizes either a conventional pulverized coal wall burner or a slagging cyclone burner. In either case the resulting ash is very different from that produced in a PFBC. Because the Tidd operation ended in March, 1995, a better simulation of the PFBC environment was sought. The 55 MWe atmospheric pressure circulating fluid bed (CFB) combustion unit located at

Ebensburg, PA was selected because it provided a good simulation of the atmosphere and ash characteristics of a PFBC. Access to this unit by MTI was facilitated because B&W was the OEM for this unit and is the partial owner. The primary disadvantage of the Ebensburg CFB was the high velocity and high ash loading of the gas stream which would require careful erosion protection of the samples. A side view of the CFB shown in Figure 5 identifies the sample locations.

Since the Ebensburg CFB was a utility power plant, it was not possible to shut the unit down to install and retrieve samples. Figure 6 shows the sample probe that was designed to be installed through standard observation ports in the side wall of the CFB while the boiler was on-line. The outer assembly was fabricated from solid and perforated 304 stainless and was intended to protect the sample from excessive erosion by the heavily ash loaded gas stream of the circulating fluid bed combustor. Also shown in Figure 6 is the inner support tube and sub-scale sample. The inner support tube was required for additional structural support of the assembly and to transfer a spring load to the flange to prevent vibration. Note that the sample flange is smaller in diameter than the conventional candle filter design because of the size constraints of the available observation ports. Prior to sample probe insertion, low-pressure air was injected into the port to prevent the escape of the combustion gas stream. Gas stream temperatures were in the 815 to 885 °C range at the time of sample insertion with no sample preheating. Considering the highly effective heat transfer of the CFB gas stream, sample insertion produced nearly instantaneous heating and was likely the most severe part of the test exposure. Likewise, at the end of the exposure period, the samples were simply pulled from the ports into ambient air. During the exposure period, the ash/sorbent was expected to penetrate the perforated tube section of the probe and accumulate around the sample. The test duration was extended to 250 hours because the originally scheduled 100 hours was considered too short to cause significant alteration of the sample properties to allow a realistic evaluation of the different bond systems or fibers included in the four test compositions.

## 6.3 Results and Discussion

### 6.3.1 Permeability

As-fabricated and post exposure test permeability results for the sub-scale elements are shown in Tables 4. As expected, the post-test samples produced higher pressure drops as a result of ash build-up on the exterior surface of the sample.

### 6.3.2 C-ring Strength

A summary of the high temperature C-ring results for the as-fabricated sub-scale samples is given in Figure 7. Composition C1 exhibited relatively low strength but with an extended strain at near maximum load. Note that the strength is not necessarily an inverse function of permeability for the boehmite-bonded compositions. The explanation is given in the section on microstructure and is related to the distribution of the bond phase. Composition C2 produced a very brittle fracture behavior in the as-fabricated condition. The brittle fracture behavior may be related to the amount of bond phase in the particular samples tested in the as-fabricated condition. Composition C3 exhibited high strength and relatively non-brittle fracture behavior. The contrast in failure behavior between composition C3 and C2 is not fully understood since the only difference between these compositions is the amount of carbon coated fiber. The compressive C-ring results for composition C4 are very similar to C1 in terms of maximum strength and failure behavior. As discussed above for composition C1, a non-uniform distribution of the boehmite bond phase appears to account for the low observed strength.

Figure 8 summarizes the C-ring results for the samples taken from the 816 °C region of the CFB. Composition C1 increased strength by approximately 16 percent compared to the as-fabricated condition and maintained good failure behavior. Composition C2 retained approximately 80 percent of the as-fabricated strength and showed a significant improvement in failure behavior as a result of the CFB exposure. Composition C3 retained 69 percent of the as-fabricated strength and continued to exhibit good failure behavior. The compressive C-ring

strength of composition C4 increased by about 47 percent and displayed a non-catastrophic failure behavior.

The high temperature C-ring results for the samples located in the 885 °C region of the CFB are shown in Figure 9. These results are very similar to 816 °C CFB samples. Composition C1 increased in strength by about 21 percent with a non-brittle type of failure. Composition C2 retained approximately 74 percent of its as-fabricated strength and also exhibited non-brittle failure behavior. Composition C3 exhibited a strength retention of about 70 percent with a non-brittle failure. Composition C4 showed the highest increase in strength of this group of samples, 73 percent with a non-brittle failure.

The post-test high temperature C-ring results for CFB thermal fatigue samples are shown in Figure 10. These samples received approximately 1000 back pulses and were located in the 816 °C region of the CFB. The composition C1 sample showed a 25 percent increase in strength with a relatively non-brittle failure. The composition C2 sample retained 80 percent of the as-fabricated strength and exhibited an extended strain past peak stress. Composition C3 exhibited a retained strength of 72 percent and produced the most extended stain at near peak stress. Composition C4 increased in strength by about 18 percent and also exhibited an extended stain at near peak stress.

In order to illustrate the effects of the various exposure conditions, high temperature C-ring results for a single composition are summarized in Figure 11. The stress versus strain results for composition C3 include the as-fabricated and the three CFB exposure conditions. As discussed above, the CFB exposure resulted in decreased strength but with high apparent toughness as indicated by the ability to sustain a near maximum load at strains approaching 0.8 percent extension.

### 6.3.3 Microstructure

In general, the SEM examination revealed very little evidence of ash or sorbent penetration into the samples following the thermal fatigue test exposure in the CFB. Figure 12 is

a 20X back scattered electron (BSE) micrograph of sample C1-4. The distribution of the Almax fiber tows appears to be relatively uniform but widely spaced due to the large number of filaments in each tow. The distribution of the boehmite bond phase appears to be more concentrated near the outside (i.e. the right side of this figure) and may have contributed to the low strength and low permeability of these samples. The observed binder distribution was attributed to migration of the liquid sol to the hot outer surface of the element where the excess water evaporated causing an accumulation of the boehmite bond phase. A more uniform distribution of the bond phase should allow increased binder contents and the associated higher strength with less of an impact on the permeability. Figures 13A and 13B illustrate the distribution of the boehmite within an Almax fiber tow. The boehmite appears as a lighter gray compared to the mount material. At 2000X, Figure 13B, the granular texture of the polycrystalline Almax fiber is apparent. Figures 14A and 14B illustrate the higher concentration boehmite bonded chopped fiber near the exterior surface of the sample.

The overall microstructure of composition C2 is shown in the 20X BSE micrograph in Figure 15. Note the lack of bond phase concentrations or gradients compared to composition C1 described above. Sections of very low or no Saffil concentration appear under some of the Nextel fiber tows. The uneven surface of the winding will likely result in gaps under the fiber tow that will not be filled with chopped fibers. That is, the continuous fiber tows shadow or block the deposition of chopped fibers. The distribution of continuous fiber tows depends on the location of the polished section surface since the winding pattern has a very coarse node distribution. Figures 16A and 16B illustrate the bonding within the Nextel 610 fiber tow near the center of the cross-section. At higher magnification, Figure 16B, revealed no evidence of fiber degradation or reaction with the bond phase. Figures 17A and 17B illustrate the distribution of chopped fiber and bond phase near the inside diameter of the sample.

Figure 18 is a 20X BSE micrograph of sample C3-2 following the CFB thermal fatigue test exposure. The increased concentration of Nextel 610 is apparent in this sample. The distribution of continuous fibers appears more uniform at the 2:1 Nextel to Saffil ratio. The microstructure is otherwise similar to C2 in terms of there being no evidence of bond phase concentration gradients. Low concentrations of chopped fiber are also visible under some of the

continuous fiber tows. Figures 19A and 19B show the distribution of the bond phase within a Nextel 610 fiber tow near the center of the sample cross-section. Figures 20A and 20B show the distribution of bond phase within the chopped fiber near the inside diameter of the sample.

The cross-section of sample C4-4 following the CFB thermal fatigue exposure test is shown in Figure 21. The bond phase concentration gradient from OD to ID (i.e. from right to left) is very similar to that observed in composition C1. Figures 22A and 22B show a lack of bond phase in the Nextel 610 fiber tow located near the inside diameter of the sample. Figures 23A and 23B show the distribution of the boehmite bond phase within the chopped fiber near the outside diameter of the sample. There appears to be good potential to improve the properties of this composition if the bond phase can be distributed more uniformly.

#### **6.4 Conclusions and Recommendations for Full-scale Elements**

Based on the mechanical properties, permeability, and the microstructure results described above, composition C3 was selected for the full-scale fabrication and simulated PFBC testing and characterization. The advantages of composition C3 include the following:

- uniform bond phase distribution
- good strength
- non-catastrophic fracture behavior for all test conditions

The disadvantages of composition C3 include increased cost as a result of the increased continuous fiber content and the added complexity of the fiber coating process and finally, the inert atmosphere heat treating required to protect the carbon fiber coating.

## **7.0 FULL-SCALE FILTER ELEMENTS: ONE METER ELEMENTS**

### **7.1 Vacuum Winding**

The capacity of the slurry handling equipment (tanks, water trap, and vacuum pump) was increased to accommodate the increased slurry volume required for the one meter long elements. The increased length actually resulted in increased winding speed and improved preform quality because the winder was not limited by the allowable acceleration on the various axes. On the sub-scale elements, the winder was essentially kept in the "turning mode" which was too slow for good distribution of the slurry. In addition, the new conical mandrel end resulted in less fiber slippage and more uniform distribution of the continuous fiber.

### **7.2 Bonding**

The vacuum wound preforms were saturated with phosphoric acid and excess acid was removed through the vacuum system. A low temperature heat treatment (538 °C) was used to cure the phosphate bond. The carbon fiber coating was removed in the final heat treatment to 927 °C in air that also converted the bond to the  $\text{AlPO}_4$  phase.

### **7.3 Flange Machining Issues**

After the final heat treatment, the built up flange section of the element was machined to the Westinghouse flange configuration. An example of the machined flange is shown in Figure 24. In the tapered section of the flange the Nextel continuous fibers were cut leaving little or no anchoring to the body of the element. A qualitative flange test was performed to estimate the resistance to clamping or mounting loads. The flange test configuration is shown in Figure 25 along with a typical load versus displacement plot. A shear failure occurred at the base of the machined flange, and a reduced bolting load was recommended to Westinghouse for the HTHP test.

## **7.4 W-STC HTHP Test**

Four composition C3 elements were evaluated in the Westinghouse High-Temperature High-Pressure (HTHP) filter test facility. The elements received 87 hours of steady state operation at 843 °C and 150 psig. In addition, the elements were subjected to a 19-hour accelerated back pulsing segment consisting of 383 back pulses and a 9 hour thermal transient test segment consisting of 6 transients. At the completion of the HTHP test exposure, all filter elements remained intact. Two of the four test elements exhibited gasket leakage due to the reduced bolting load. The test elements were returned to MTI for mechanical and microstructural characterization.

### **7.4.1 Filter Issues**

Based on the HTHP testing, Westinghouse recommended the following component modifications:

- Increase flange strength
- Increase length to at least 1.5 meters
- Increase permeability

## **7.5 Results and Discussion**

### **7.5.1 Composition**

The composition of the six elements prepared for the Westinghouse HTHP test is shown in Figure 26. This composition corresponds to composition C3 in Table 3.

### **7.5.2 Permeability**

Sample permeability is determined from the pressure drop across the element measured at a face velocity of 10 ft/min. As shown by the lower curve in Figure 26, all six samples prepared

for this test exhibited higher pressure drops than the Westinghouse specification of less than 10 in wg at 10 ft/min.

### 7.5.3 C-ring Strength

The compressive C-ring results for the 8/96 W-STC test of composition C3 elements are shown in Figure 27. It is apparent that all the samples exhibited non-catastrophic failure behavior. The samples exhibited a retained strength of 70% of the as-fabricated strength following the HTHP test.

### 7.5.4 Microstructure

Polished sections cut from of the Westinghouse one meter samples were examined to determine the extent of ash/sorbent penetration as well as the relative distributions of the Nextel 610, Saffil, and bond phase. Figure 28 is a 20X back scattered electron (BSE) image illustrating the full wall thickness of an as-fabricated filter element (6-6-10). The sample OD is at the top of the figure and the plane of the image is perpendicular to the element axis. The Nextel 610 flat ribbon-like morphology is apparent as is the uniform distribution of the  $\text{AlPO}_4$  bond phase. Figure 29 is a 150X BSE image that is typical of the microstructure at the 1/3 and 2/3 positions through the filter wall. Portions of four Nextel 610 tow bundles are on the left side of this micrograph and the phosphate ( $\text{AlPO}_4$ ) bonded Saffil is visible in the upper right. The uniform bond distribution observed in these samples is typical of the phosphate bond system.

An example of the post-test microstructure is shown in Figure 30, a 10X BSE image of sample 6-6-19. The morphology of the ( $\text{AlPO}_4$ ) bonded Saffil is shown in the 150X BSE image in Figure 31. No evidence of ash penetration was found in this examination. The 20X BSE image of the OD surface of sample 6-6-17 shown in Figure 32 gives a good indication of the +45° and -45° continuous fiber architecture along with the Saffil fiber matrix. Note that the gas flow is restricted to the Saffil region between the Nextel fiber tow bundles. The width of the Nextel tow clearly controls the permeability of the element at a given fiber bandwidth or separation. The 1000X (BSE) image shown in Figure 33 reveals ash/sorbent accumulations on

the Saffil fibers. Calcium, potassium, and iron were detected at location (1) by EDS analysis. Similar examination of the inside surface of filter element 6-6-17 also revealed the presence of ash/sorbent material. The presence of ash/sorbent on the ID surface was a result of the gasket leak that was reported for this sample. No evidence of coal ash penetration was found in the interior of the sample cross-section.

Examination of samples that were impregnated with thermal-plastic, cut, polished and then rinsed in acetone to remove the thermal plastic gave an excellent illustration of the vacuum wound filter microstructure. Figure 34, a 150X BSE image of sample 6-6-6, shows three Nextel 610 tow bundles laid down in consecutive passes of the filament winder and illustrates the change in direction of the winding head as it proceeds down and back along the preform. The distribution of the Saffil matrix is well represented in this figure.

## **7.6 Conclusions and Recommendations**

The primary issues identified in this test phase were the flange strength, low permeability of the elements as well as the high cost and equipment limitations associated with the  $AlPO_4$  bond system. Each of these issues was resolved in the Filter Improvement and Cost Reduction phase of the program.

## **8.0 FILTER IMPROVEMENT AND COST REDUCTION**

Continued process development focused on the following aspects:

- shape of the Nextel fiber tow bundle
- relative distribution of the Nextel and Saffil fibers
- flange strength
- development of an alternate bond phase that would eliminate the need for fiber coating and inert atmosphere heat treatments

### **8.1 Vacuum Winding**

#### 8.1.1 Nextel Fiber Shape

As discussed above, the ribbon-like shape of the Nextel 610 fiber tow contributed to the low permeability of the elements. Discussions with the supplier, 3M, indicated that the rayon served version of the fiber would be more compact and circular in cross-section. The specific rayon serving consisted of 8 to 10 turns/inch in the S direction. Figures 35 and 36 clearly illustrate the difference in cross-section between the standard Nextel 610 and the rayon served fiber, respectively. Test samples vacuum wound with the rayon served fiber exhibited significantly higher permeability as a result of the more compact fiber tow. In addition, the handling strength and winding behavior of the rayon served fiber were noticeably better compared to the standard sized fiber. Based on these results, all subsequent filter elements were fabricated with rayon served fiber.

#### 8.1.2 Fiber Architecture

In an attempt to optimize the utilization of the expensive Nextel fiber, the slurry feed rate was varied to control the relative amounts of Nextel 610 and Saffil throughout the wall thickness. The shortest winding times were achieved by controlling the slurry feed rate, however, the same result could be achieved by controlling the winding speed. An example of the controlled

distribution of fiber is illustrated in Figure 37 which plots the Nextel and Saffil fiber contents for each winding closure or layer from the ID to the OD. As shown in the figure, the relative amount of Nextel fiber is greater in regions of increased stress near the OD and ID surfaces and decreased in the mid-wall region. It is important to note that other distributions may be desired depending on the mechanical or thermal environment. The capability to control the fiber distribution is unique to the vacuum winding process.

### 8.1.3 Net Shape Flange

As discussed above, producing the required flange contour by machining a built up section destroys much of the advantage of a fiber-reinforced structure. Therefore, a net shape flange was produced during the vacuum winding process by contouring the wet preform to the desired shape. The resulting flange shown in Figure 38 requires no further machining and is an integral part of the filter element. The reinforcement fibers remain intact from the body to the flange region and provide an effective transfer of bolting loads instead of relying on the shear strength of the wound structure. Elimination of the machining step not only saves a significant amount of labor but also avoids the potential for air borne fibers.

## 8.2 Bonding

The boehmite bond system was re-examined as an alternative to the phosphoric acid bond system in order to simplify the processing and to eliminate the need for inert atmosphere heat treatments. The study focused on stabilizing the boehmite sol within the structure in order to prevent drying induced migration to the outer surface. The first approach used ammonia gas to gel the sol by increasing the pH. Vacuum formed Saffil fiber pads were saturated with the boehmite sol and ammonia gas was drawn through the pads to initiate gelling. SEM examination of the dried and fired pads revealed relatively uniform bond phase distribution. Application of the ammonia gas gelling step to the vacuum wound preform resulted in low permeability. Apparently, the gelled sol formed a film that decreased the permeability. Note that this study was performed before the use of served fiber or the controlled fiber distribution.

An MTI developed inorganic polymer bond system was also studied. The aluminum nitrate based polymer was developed for final densification of dense composites on the CFCC program. Preliminary tests on vacuum wound preforms produced unacceptable strengths (~200 psi) and the approach was abandoned.

### **8.3 Results and Discussion**

#### **8.3.1 C-ring Strength and Permeability**

The compressive C-ring strength of boehmite bonded samples prepared with the controlled fiber distribution is shown in Figure 39. Even at the reduced level of Nextel fiber that resulted from the controlled fiber distribution winding, the C-ring strength was over 1200 psi. Note that the served Nextel fiber was not yet available when this testing was performed.

### **8.4 Conclusions and Recommendations**

Based on these results, the rayon served Nextel 610 fibers, the controlled distribution vacuum winding process, the boehmite bond, and the net shape flange were selected for the 50 Filter Element Option. The boehmite bond was utilized because it was necessary to eliminate the fiber coating and inert atmosphere heat treatments in order to simplify the process and reduce costs. It was recognized that additional work was needed to optimize the boehmite bond distribution.

## **9.0 FABRICATION OF 50 ELEMENTS FOR TESTING: KARHULA PCFB TEST**

Twelve filter elements were fabricated for testing at the Foster-Wheeler pressurized circulating fluid bed combustor (PCFB) located in Karhula, Finland. These elements were fabricated using rayon served Nextel 610, the controlled fiber distribution, net shape flange, and the boehmite bond system discussed above.

### **9.1 Results and Discussion**

#### **9.1.1 Composition and Permeability**

The compositions and permeabilities of the 12 full size filter elements submitted for the TS2-97 test campaign in the Foster-Wheeler pressurized circulating fluid bed (PCFB) facility in Karhula, Finland are shown in Figure 40. These results demonstrate the consistency of the fabrication process. Six MTI filter elements were installed at the start of the run and completed 581 hours of coal testing without failure. A seventh element completed 342 hours without failure. Details of the test campaign are given in Table 6.

#### **9.1.2 Surface Defects**

During a mid-run inspection, surface defects were observed on some of the MTI elements. A typical defect is shown in Figure 41 and consisted of 1 to 2 cm<sup>2</sup> regions of missing Saffil. Inspection of an as-fabricated element revealed similar defects and it was concluded that the defects were due to a manufacturing problem and not caused by the test exposure. The Foster Wheeler operators also noted that a substantial quantity (~70 g) of ash/sorbent was found on the inside of some of the MTI elements. This was attributed to leaking gaskets on blanked off elements and/or leaking fail-safes. Since the MTI filter element does not utilize a filtration membrane, neither the surface defects nor the ash on the inside of the element would be expected to degrade the filtration effectiveness of the element.

### 9.1.3 C-ring Strength

The C-ring load versus displacement results for the as-fabricated and PCFB tested elements are shown in the upper and lower portions of Figure 42, respectively. The non-catastrophic failure behavior of these samples is apparent in this figure. Additional C-ring tests were performed on samples prepared with the surface defect described above located in the high stress position to determine the effect of the defect on element properties. After 581 hours of testing in the Karhula facility, the filter elements retained approximately 87% of the as-fabricated strength and continued to exhibit non-catastrophic failure behavior.

## 9.2 Conclusions and Recommendations

Three of the elements from the Karhula test were included in the PSDF test for additional run time. The remaining Karhula elements were returned to Westinghouse for accelerated back-pulsing and thermal transient testing. Based on these results, additional elements were fabricated for testing in the PSDF.

## **10.0 FABRICATION OF 50 ELEMENTS FOR TESTING: PSDF TEST**

Thirteen filter elements were fabricated for testing in the M. W. Kellogg module at the PSDF using the same composition as the Karhula elements. In addition, three of the Karhula elements were also included in PSDF test runs TC02 and TC03. A summary of the filter element run time at the PSDF is given in Table 7. A summary of all filter testing to date is given in Table 8.

### **10.1 Results and Discussion**

#### 10.1.1 Composition and Permeability

The composition and permeability of each of the filter elements shipped to the PSDF are included in Figure 43. As shown on the table, both the composition and permeability were very consistent for this production lot.

#### 10.1.2 PSDF TC02 Thermal Excursion

At the start of TC02, a severe thermal excursion occurred during the transition from the start-up burner to coal firing. Apparently, unburned coal carried over to the filter vessel and deposited on the elements. As the vessel continued to heat up, the coal ignited on the element surface and resulted in several failures of the monolithic oxide elements. Thermocouples mounted on selected elements indicated a thermal gradient of about 350 °F across the element wall. All 9 MTI elements survived this thermal excursion. Although operation improvements have been implemented, coal feed problems are not likely to be eliminated completely and this type of thermal excursion must be considered in the future selection of elements.

## **11.0 CFCC MODELING AND TESTING SUPPORT**

As part of the CFCC program, the Material Response Group at Virginia Tech developed a ligature model<sup>8</sup> of the vacuum wound composite material and performed mechanical testing on filter elements. Test methods were also developed for burst (hoop), tensile, and three point bending. In addition, the mechanical response of filter element 7-6-4 from the Karhula test was characterized by applying a cantilever load to a mounted flange section of an element (approximately 30 cm long) in the configuration shown in Figure 40. The load was applied approximately 20 cm from the mounting collar. The photograph in Figure 40 illustrates the non-catastrophic failure behavior of the flange section of the element at a maximum deformation of about 25 mm. The failure occurred in the compression surface (top surface in the photo) of the element approximately 25 mm from the mounting collar. Note that the element remained intact even at the considerable deflection produced in this test. Failures of this type occur because the Nextel 610 fiber has not been degraded during the 581 hour Karhula test and continues to hold the structure together. The corresponding load versus deflection plot also shown in Figure 40 is an example of the data that will be used to validate the Virginia Tech structural model. These results clearly demonstrate the inherent strain tolerance of the vacuum wound MTI elements. Monolithic filter elements would not survive deformations of the type without catastrophic failure.

## **12.0 CONCLUSIONS AND RECOMMENDATIONS**

### **12.1 Benefits of the MTI Vacuum Wound Filter Element**

This program has demonstrated a hot gas filter concept and a flexible fabrication method to produce an oxide-oxide composite based filter with improved strength and toughness compared to monolithic filter materials. The high alumina composition is expected to be stable in both combustion and gasifier environments. In addition, the flexibility of the process in terms of the fiber distribution provides a method to optimize performance and/or cost. The combination of a low elastic modulus and non-catastrophic failure behavior results in a very rugged element that is extremely tolerant of both mechanical and thermal upsets. Finally, the process should easily scale up to longer filter elements (e.g. 2 meters or more) since the initial bonding is performed on the mandrel. The combination of low preform weight and good intermediate strength results in good handling strength. Utilization of longer filter elements provides an efficient way to increase the filtration area of the system. Furthermore, the light weight elements (i.e. ~ 1.1 kg) would result in a significant total weight reduction of about 3000 kg for a 750 element filter vessel compared to monolithic SiC elements.

### **12.2 Development Status and Manufacturing Scale-up**

The status of the MTI hot gas filter fabrication process is shown in Table 9. The major filter challenges are related to manufacturing scale-up and cost. Process scale-up will require a multi-spindle filament winder along with larger dryers and ovens. The cost of the MTI filter element is dominated by the current cost of the 3M Nextel 610 fiber. It is expected that the fiber cost will decrease significantly as production volume increases. Alternate fibers also need to be examined to reduce the cost of the raw materials.

As the filter market develops, the BWXT division of McDermott will set up a manufacturing facility in Lynchburg, VA. The Babcock & Wilcox Power Generation Group will perform marketing and distribution activities.

### **12.3 Future Work**

Additional testing will be performed in the PSDF Kellogg module and Foster Wheeler PCFB module. Potential gasifier test sites are being explored. Successful tests at these facilities are expected to lead to full-scale testing in the Foster Wheeler PCFB located at Lakeland, FL. Continued fabrication development will focus on increasing the length of the elements to 2 meters or more. The En-tec filament winder currently used in this program is limited to 1.8 meters. Initial development of the 2 meter elements would be performed on the Cobra filament winder that has a maximum bed length of over 3 meters. Finally, alternate continuous fibers need to be evaluated.

**Table 1. Open-end tube compositions.**

	C1	C2	C3	C4
<b>Continuous fiber</b>	Almax	Nextel 610	Almax	Nextel 610
<b>Continuous to chopped fiber ratio</b>	1:1	1:1	2:1	1:1
<b>Continuous fiber coating</b>	carbon*	carbon*	None	none
<b>Bond</b>	AlPO <sub>4</sub>	AlPO <sub>4</sub>	AlPO <sub>4</sub>	Thermal bonded
<b>Continuous fiber architecture</b>	45° helical	45° helical	45° helical	45° helical

pyrolyzed sizing

**Table 2. Open-end tube properties.**

	C1	C2	C3	C4
<b>Continuous fiber (wt. %)</b>	34	36	51	nd*
<b>Saffil (wt. %)</b>	35	35	28	nd*
<b>Binder (wt. %)</b>	30	28	21	nd*
<b>Pressure drop (in wg @ 10 ft/min)</b>	4.1	9.8	5.7	nd*
<b>C-ring (25 °C, psi)</b>	1651	1477	2100	nd*
<b>Tangent modulus (25 °C, msi)</b>	0.64	0.51	0.84	nd*
<b>C-ring (871 °C, psi)</b>	1139	1249	1716	nd*
<b>Tangent modulus (871 °C, msi)</b>	0.36	0.49	0.80	nd*

nd\* = not determined

**Table 3. Sub-scale candidate filter compositions.**

	<b>C1</b>	<b>C2</b>	<b>C3</b>	<b>C4</b>
<b>Continuous fiber</b>	Almax	Nextel 610	Nextel 610	Nextel 610
<b>Chopped fiber</b>	Saffil	Saffil	Saffil	Saffil
<b>Continuous to chopped ratio</b>	1:1	1:1	2:1	1:1
<b>Continuous fiber coating</b>	none	Carbon*	Carbon*	none
<b>Bond type</b>	Boehmite sol	Phosphoric acid	Phosphoric acid	Boehmite sol
<b>Continuous fiber architecture</b>	45° helical	45° helical	45° helical	45° helical

\* immiscible liquid carbon coating process

**Table 4. Properties of sub-scale hot gas filter elements**

Sample Composition	Fiber (wt.%)	Saffil (wt.%)	Bond (wt.%)	$\Delta P$ @ 10ft/min (inches H <sub>2</sub> O)		C-ring 871 °C (psi)
				pre test	post test	
As-Fabricated						
C1	38.2	41.0	20.8	6.3	nd*	825
C2	31.4	38.0	30.6	6.2	nd	1704
C3	52.6	28.1	19.3	11.9	nd	1752
C4	37.4	42.8	19.8	5.3	nd	856
CFB Exposed						
C1	36.5	40.4	23.1	5.6	10.3	995
C2	35.5	40.4	24.2	3.8	9.0	1330
C3	52.3	28.5	19.2	5.9	10.2	1228
C4	34.1	40.4	25.5	9.6	13.5	1249

nd = not determined

**Table 5. Filter element composition and fiber architecture for W-STC test in 8/96.**

Continuous fiber	Nextel 610
Chopped fiber	Saffil
Continuous to chopped ratio	2:1
Continuous fiber coating	carbon
Continuous fiber architecture	45° helical
Bond type	Phos
Flange	Machined

**Table 6. TS2-97 Test campaign at the Foster Wheeler pressurized circulating fluid bed combustion test facility in Karhula, Finland.**

<b>Date</b>	<b>September 4, 1997 - November 7, 1997</b>
<b>Number of Filter Elements Tested</b>	<b>7</b>
<b>Filter Operating Temperature, °C</b>	<b>700-750</b>
<b>Filter Operating Pressure, bar</b>	<b>9.5 -11</b>
<b>Coal Feed</b>	<b>Eastern Kentucky</b>
<b>Sorbent</b>	<b>Florida Limestone</b>
<b>Time, hrs.</b>	<b>581 (6)*, 342 (1)</b>
<b>Face Velocity, cm/sec</b>	<b>2.8 - 4</b>
<b>Particle Load, ppmw</b>	<b>6000 - 9000</b>
<b>Particle Size, μm</b>	<b>&lt;1 - 150</b>
<b>Thermal Excursions</b>	<b>None</b>
<b>Number of Startup/Shutdown cycles</b>	<b>7</b>

**Table 7. PSDF run summary.**

Number of elements	Karhula	PSDF TC02	PSDF TC03	Total Hours
3	581	559	660	1800
6	0	559	660	1219
2	0	0	660	660

**Table 8. Field exposure test summary.**

Test Facility	Filter Type	# of elements	Duration (hours)
<b>Ebensburg CFB</b>	C1, C2, C3, C4	3 of each type	250
<b>Westinghouse HTHP</b>	C3	4	100
<b>FETC Combustor</b>	C3	3	24
<b>Westinghouse HTHP</b>	C4M	1	100
<b>Karhula</b>	C4M	6	581
<b>Karhula/PSDF TC02/TC03</b>	C4M	3	1800
<b>PSDF TC02/TC03</b>	C4M	6	1219
<b>PSDF TC03</b>	C4M	2	660

**Table 9. MTI hot gas filter status.**

Property	Req't.	Status	Challenge
size	2.4 x 60"	2.4 x 60"	Complete
shape	flanged, closed end tube	closed end tube with integral flange	Complete
pressure drop @ 10ft/min	10	5	Complete
strength	1 - 4 ksi	0.8 - 1.2 ksi	Moderate
toughness	non-brittle failure	non-brittle failure	Moderate
thermal shock	survive severe plant upsets	Survived	Moderate
corrosion resistance	3 year life	Tbd	Significant
scale-up	Thousands/yr	Planning	Significant
cost	\$500-1000	Nextel fiber cost and labor cost	Significant

Figure 1. Vacuum winding schematic.

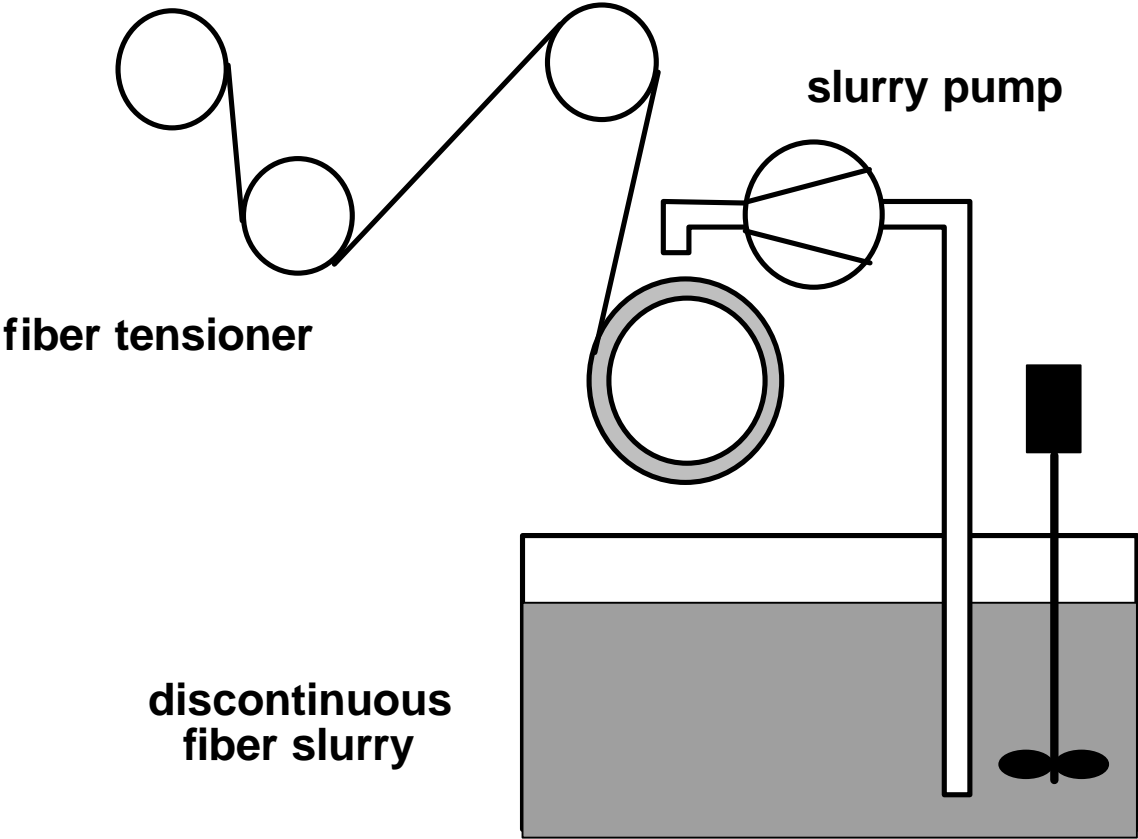


Figure 2. Composition C1 open-end tube compressive C-ring results.

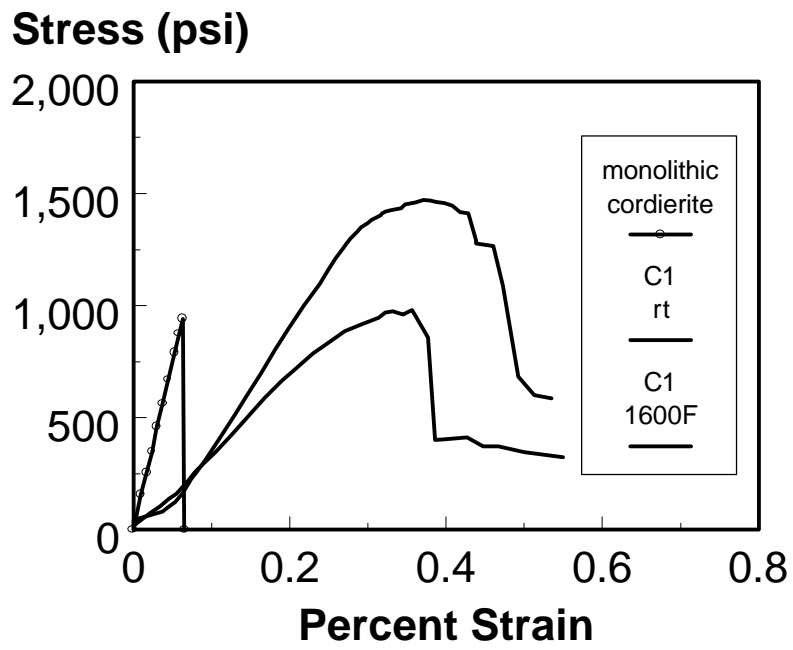


Figure 3. Composition C2 open-end tube compressive C-ring results.

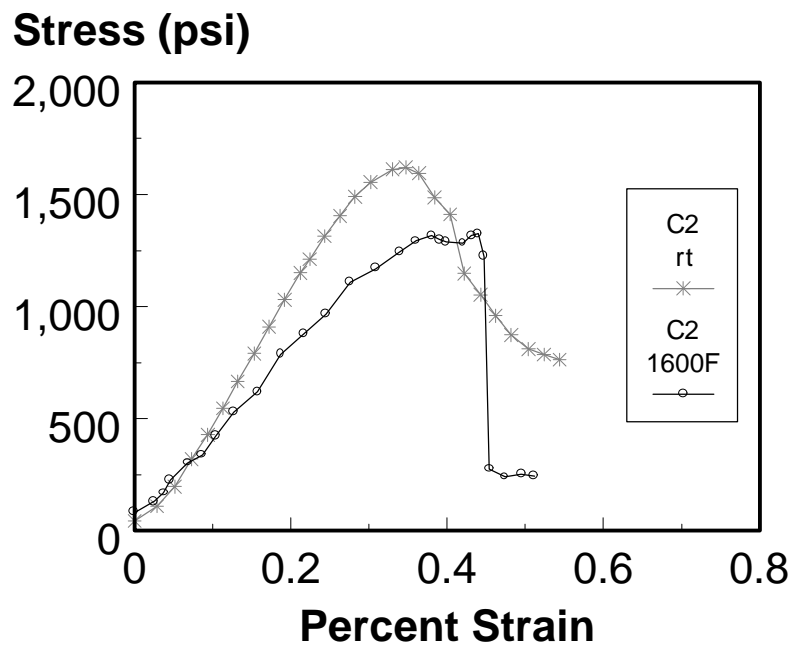
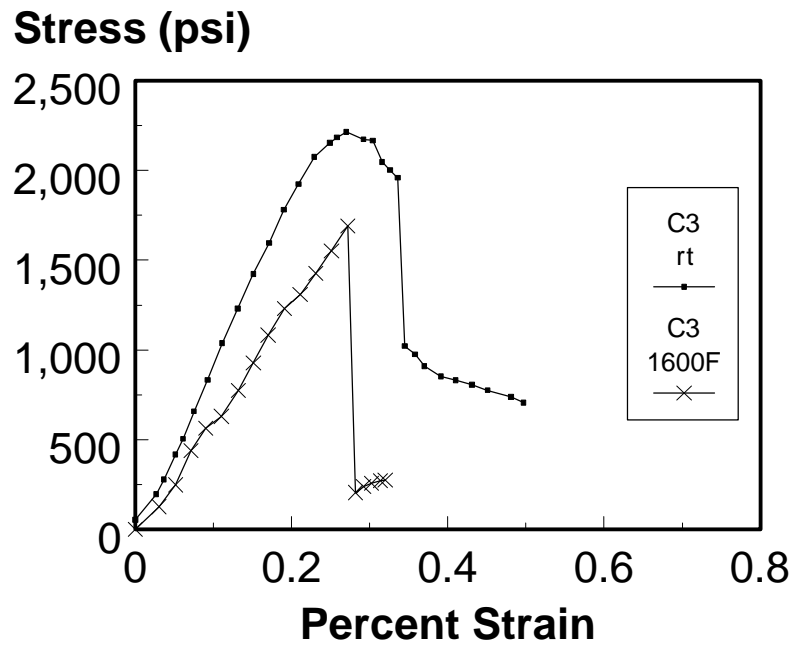


Figure 4. Composition C3 open-end tube compressive C-ring results.



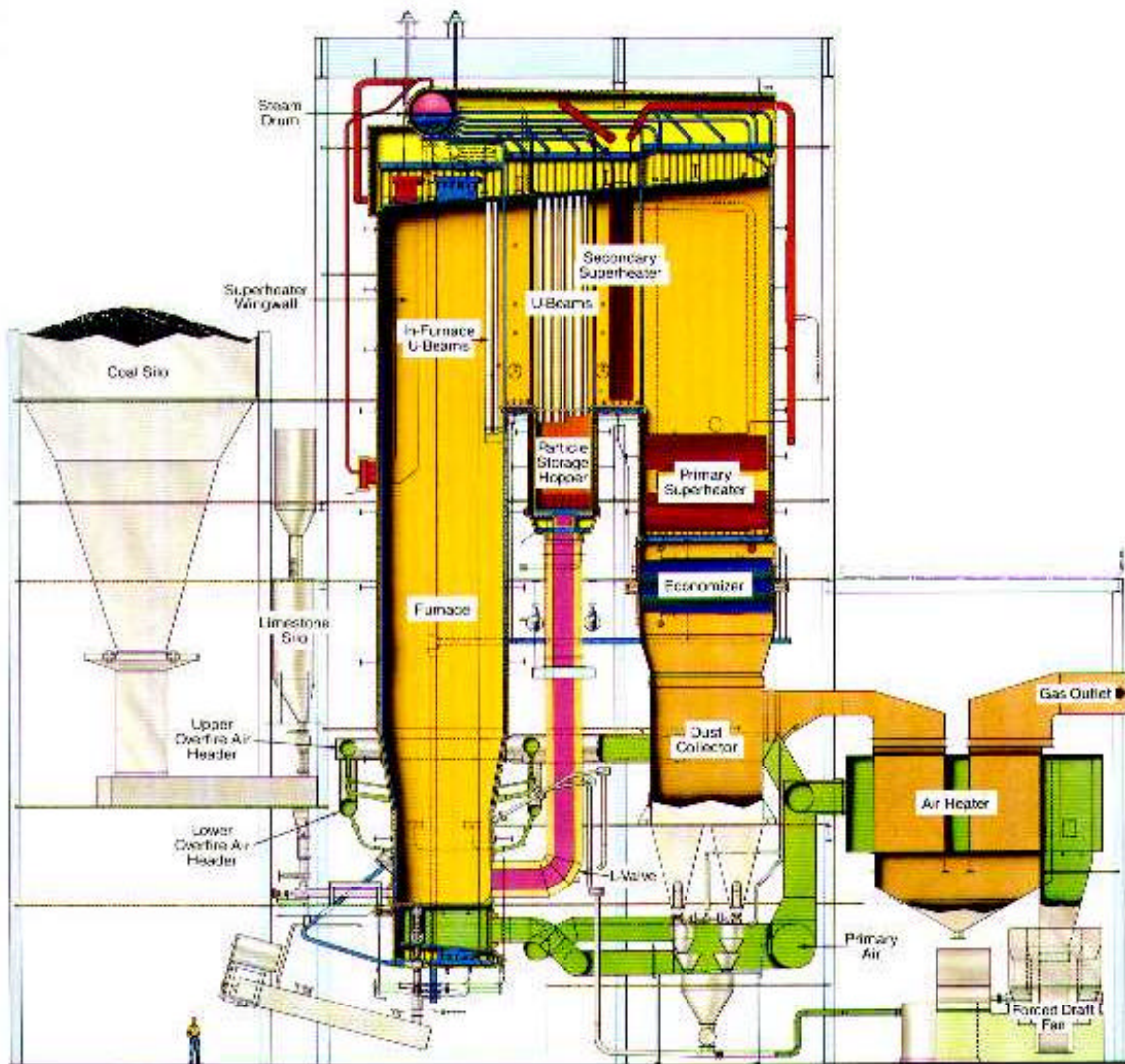


Figure 5. Ebensburg Power/B&W 55 MWe circulating fluid bed combustion unit.

Figure 6. Sample probe for sub-scale samples and observation port (below).

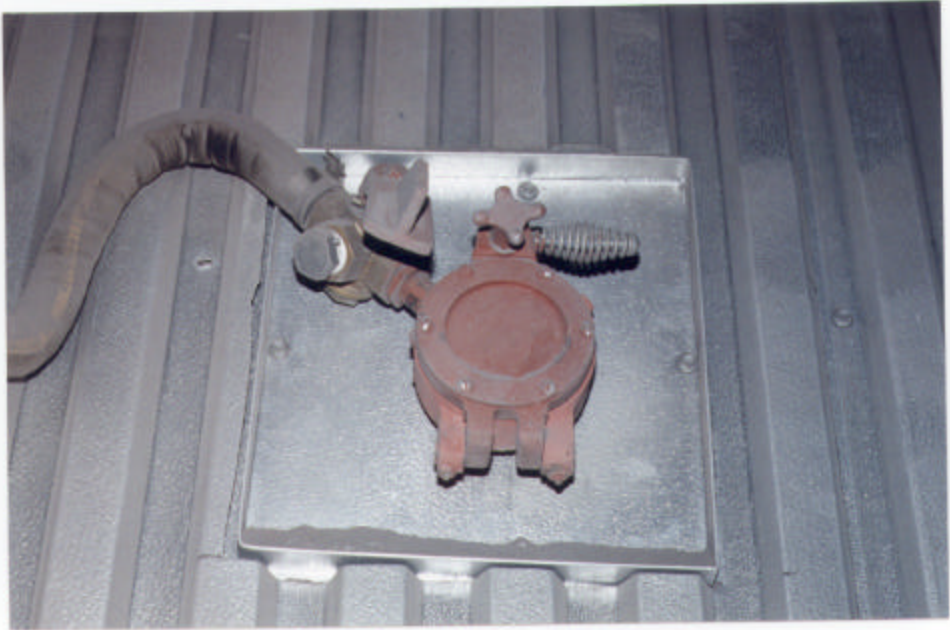


Figure 7. As-fabricated compressive C-ring results for sub-scale elements.

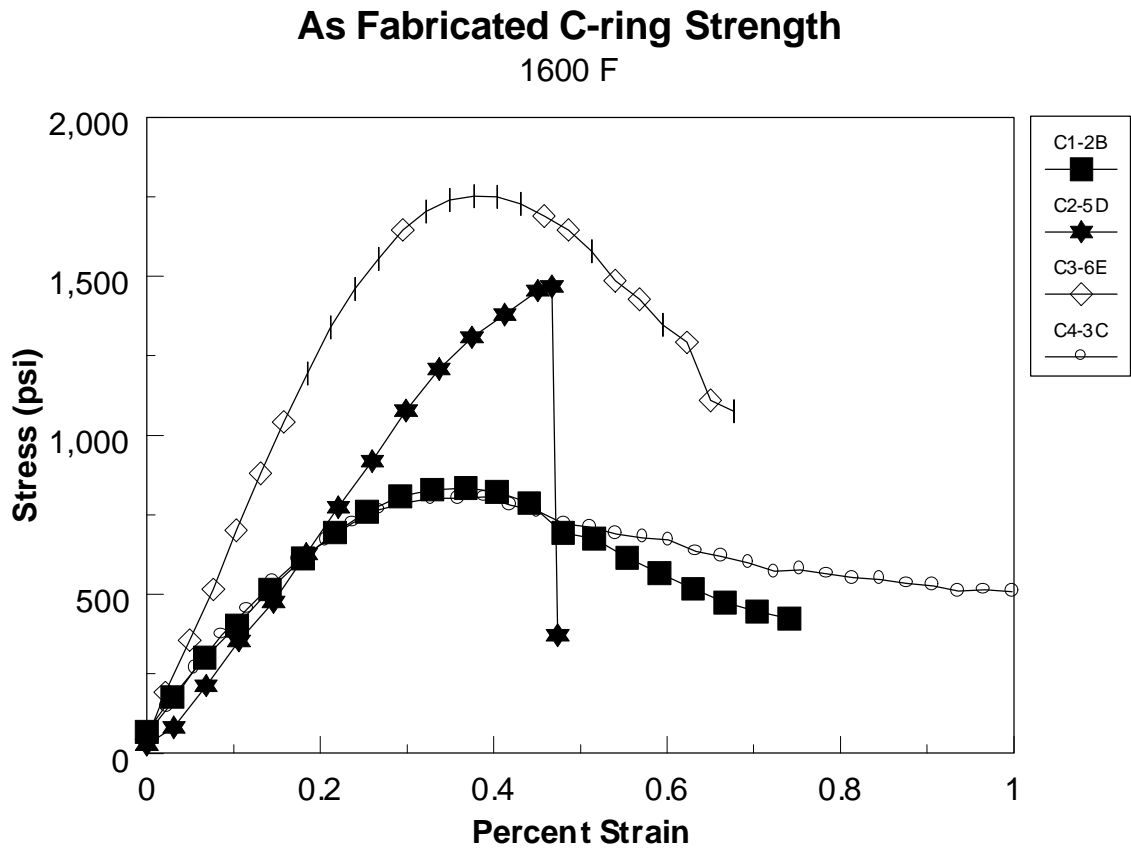


Figure 8. Compressive C-ring results for CFB (816C) samples.

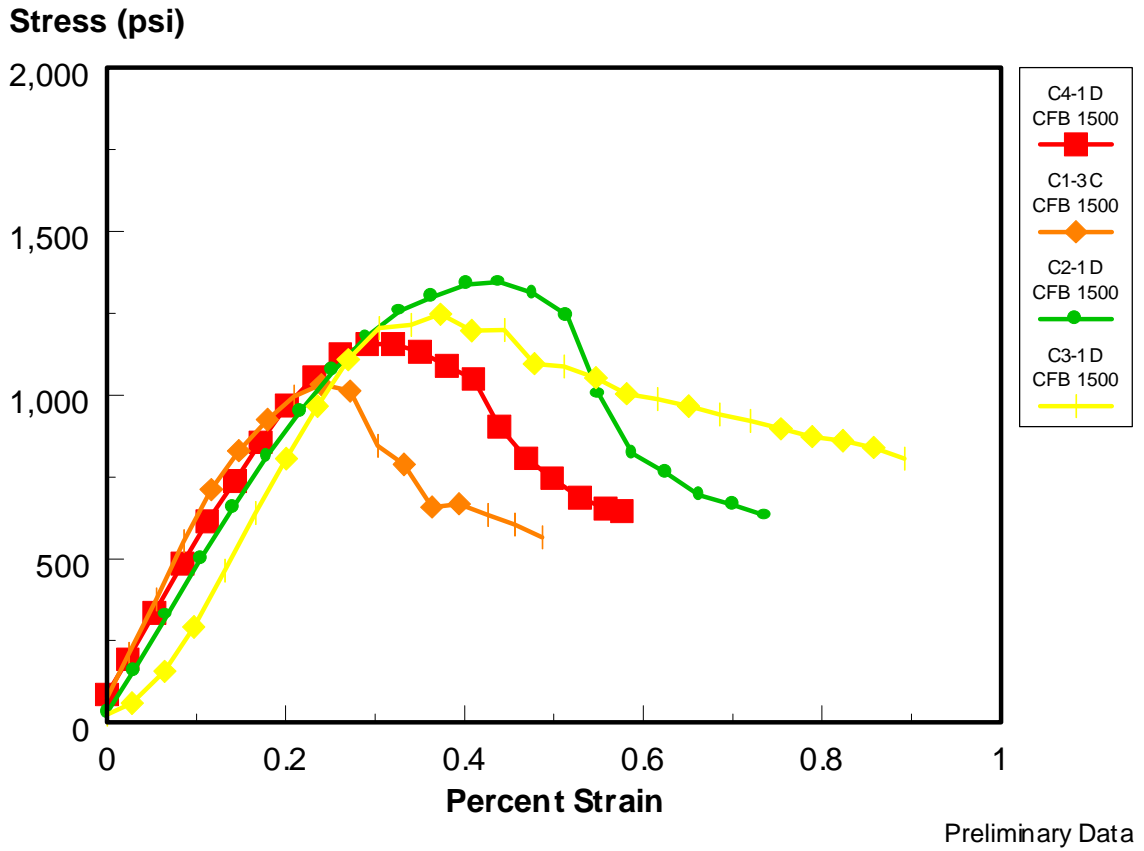


Figure 9. Compressive C-ring results for CFB (885C) samples.

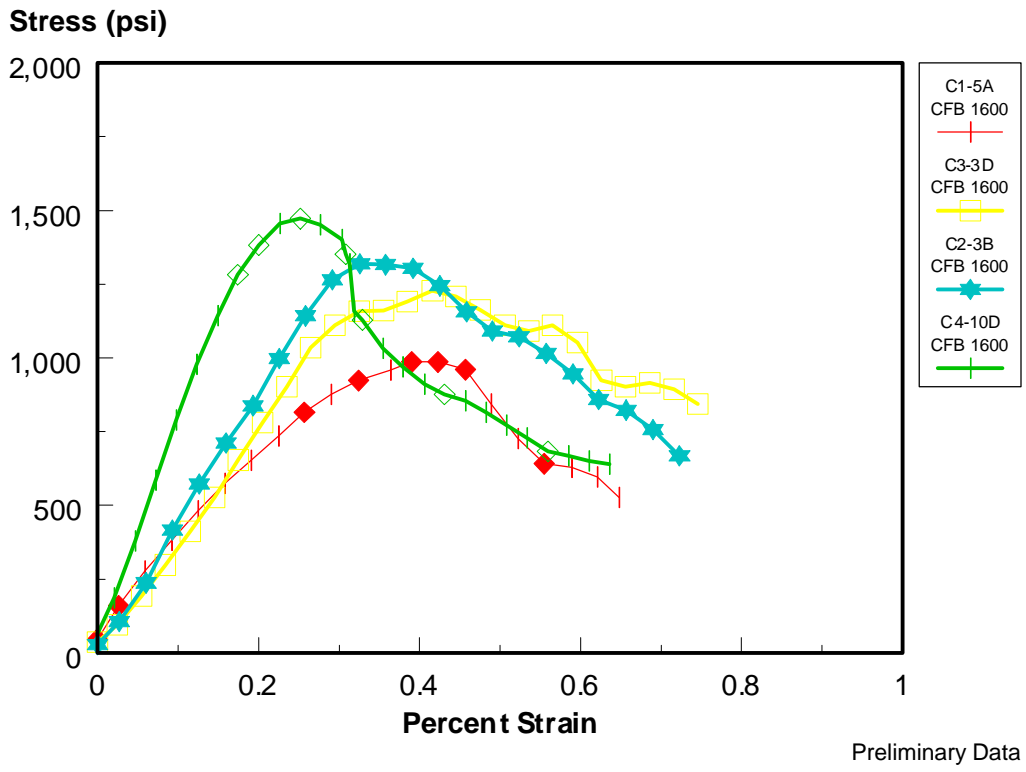


Figure 10. Compressive C-ring results for CFB fatigue samples.

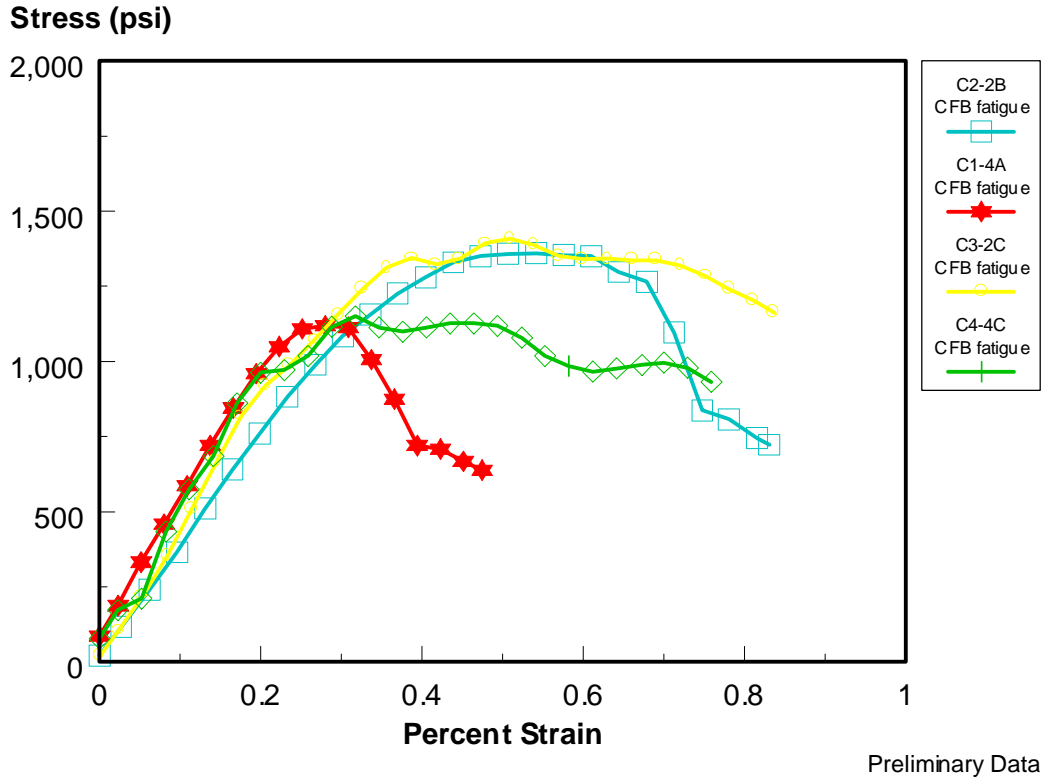


Figure 11. Summary compressive C-ring results for composition C3.

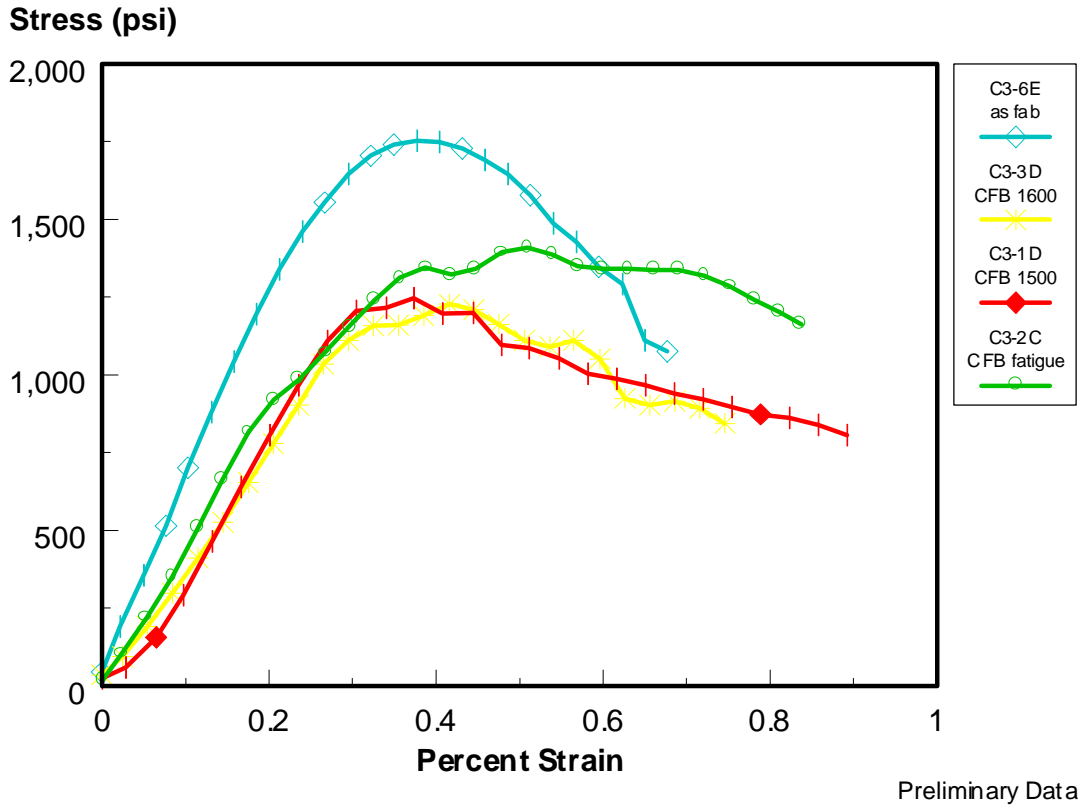
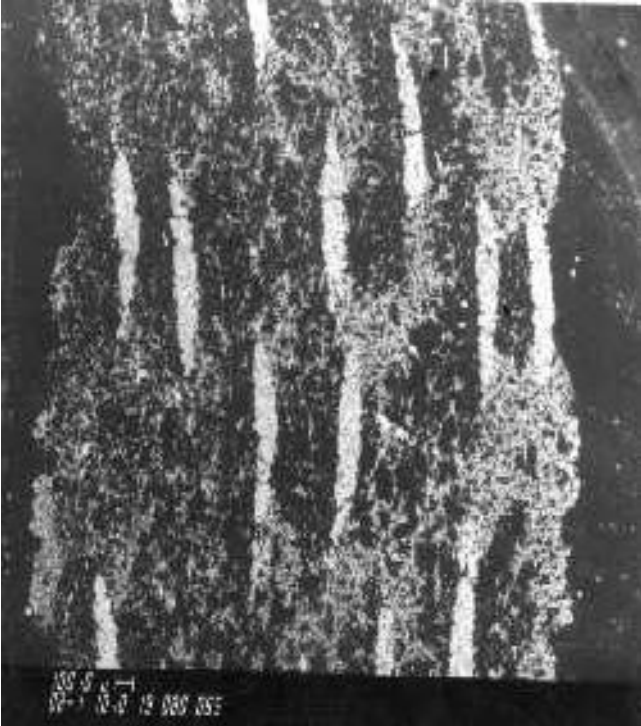
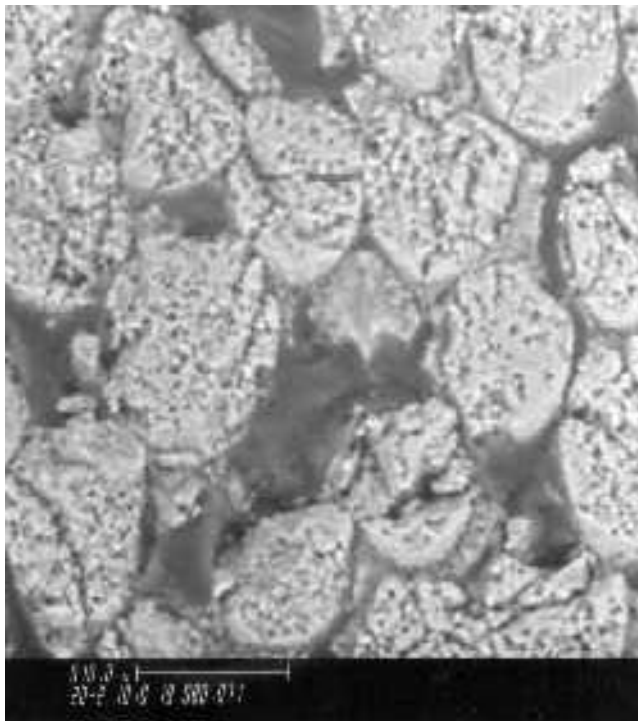
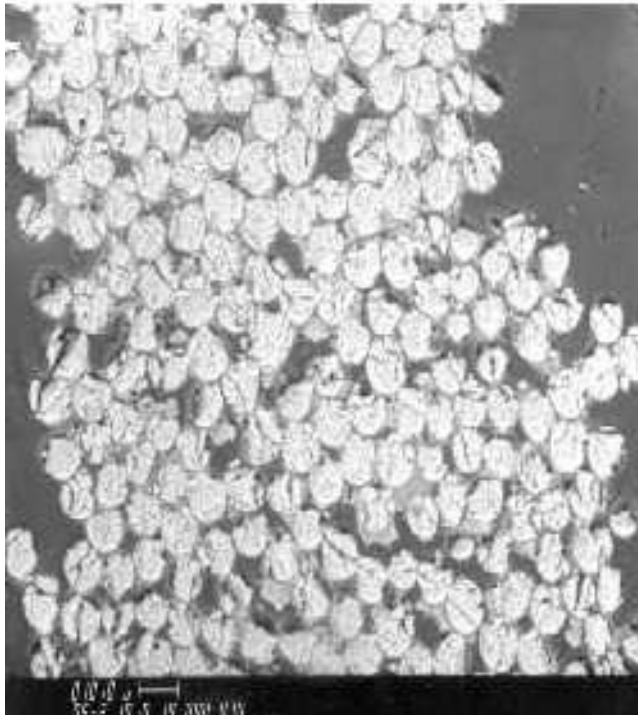


Figure 12. 20X BSE of sample C1-4.



**Figure 13. A. 500X BSE image of fiber tow bundle in sample C1-4 from CFB thermal fatigue test. B. 2000X BSE image of individual Almax fibers and bond phase from sample C1-4.**



**Figure 14. A. 500X BSE image of chopped fiber region of sample C1-4 from CFB thermal fatigue test. B. 2000X BSE of boehmite bonded chopped fiber from sample C1-4.**

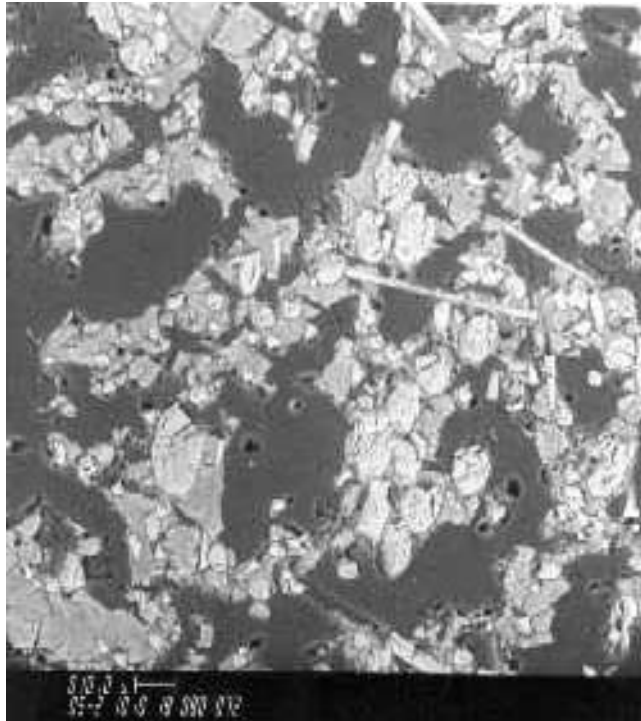
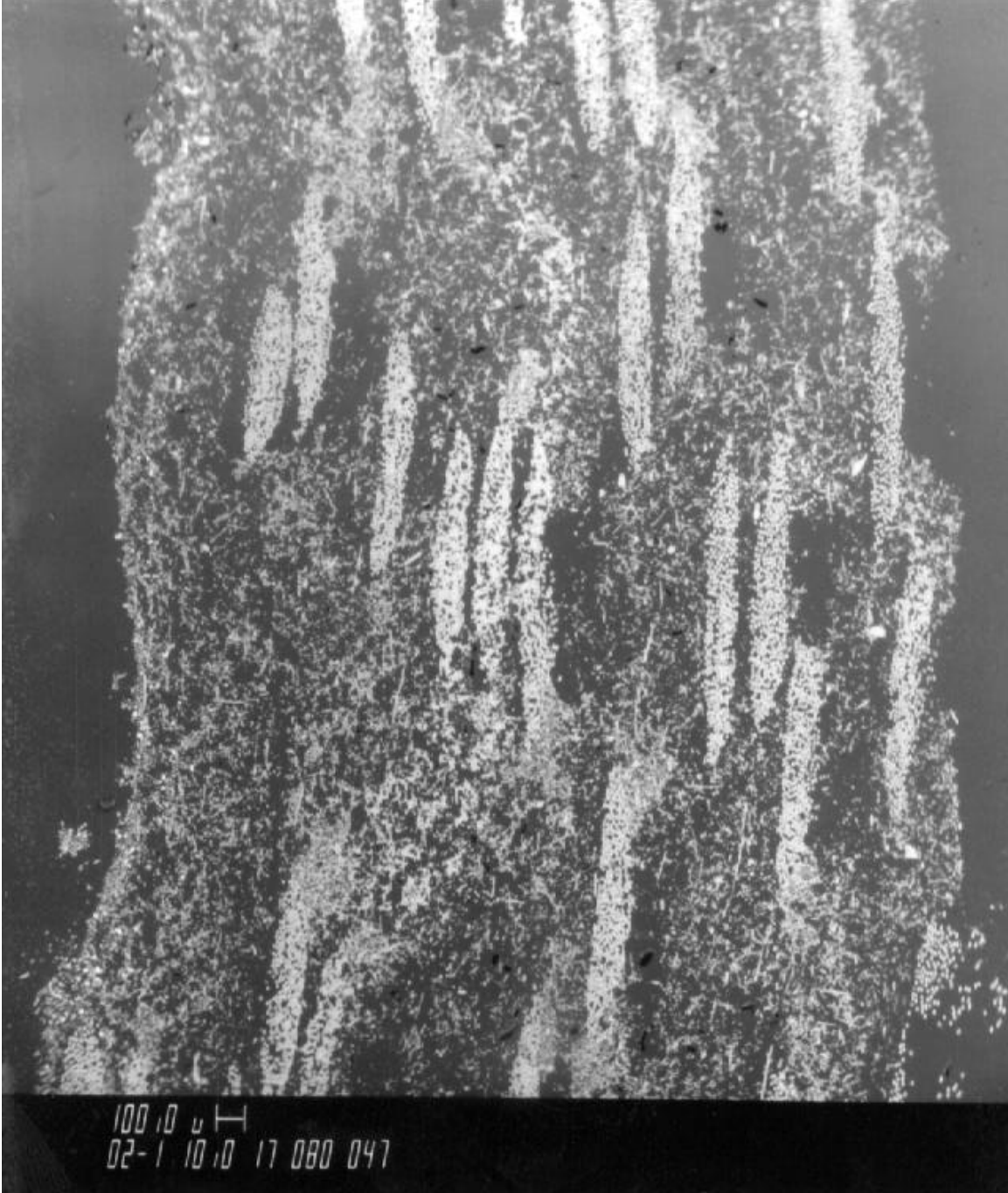
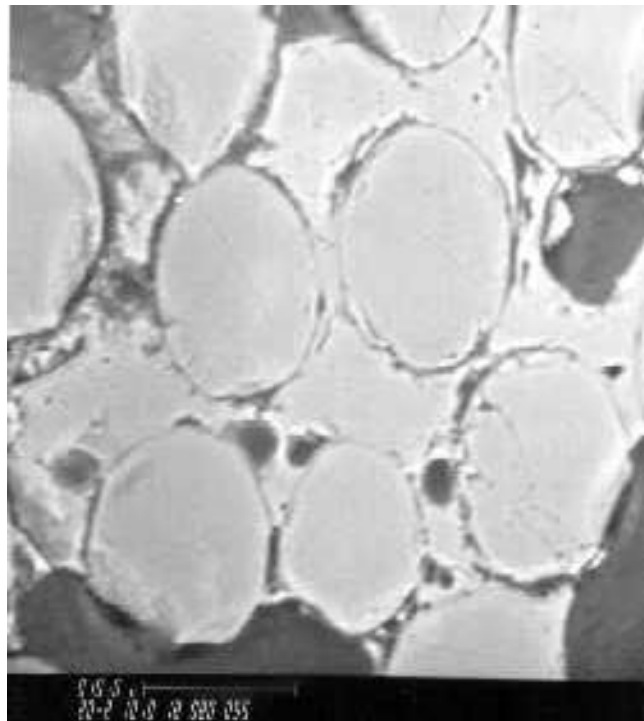
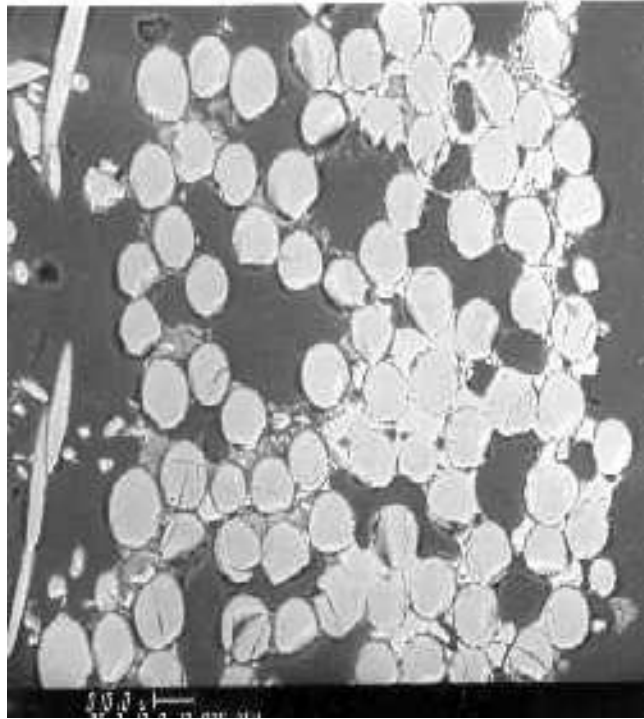


Figure 15. 20X BSE image of sample C2-2 from thermal fatigue exposure test.



**Figure 16. A. 500X BSE image of Nextel 610 fiber tow in sample C2-2 from CFB thermal fatigue test. B. 2000X BSE image of Nextel 610 fibers and bond phase from sample C2-2.**



**Figure 17. A. 500X BSE image of chopped fiber region of sample C2-2 from CFB thermal fatigue test. B. 2000X BSE image of chopped fibers and bond phase in sample C2-2.**

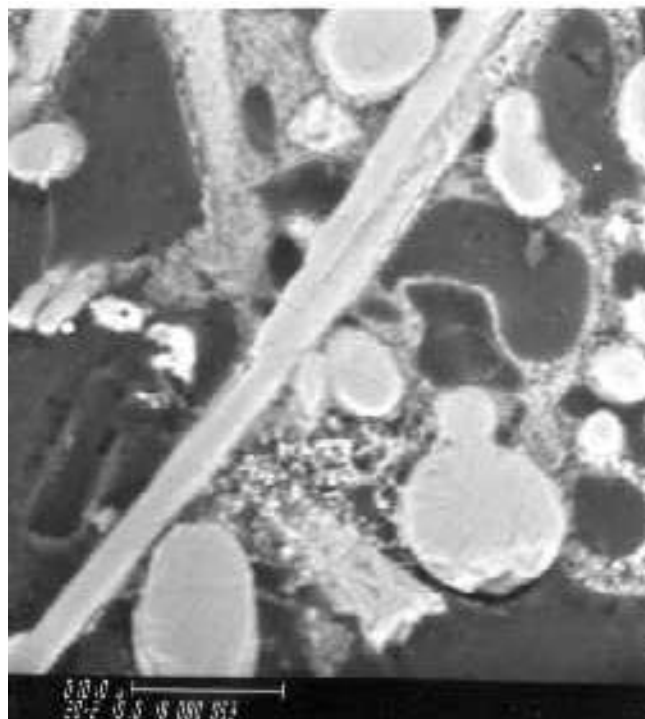
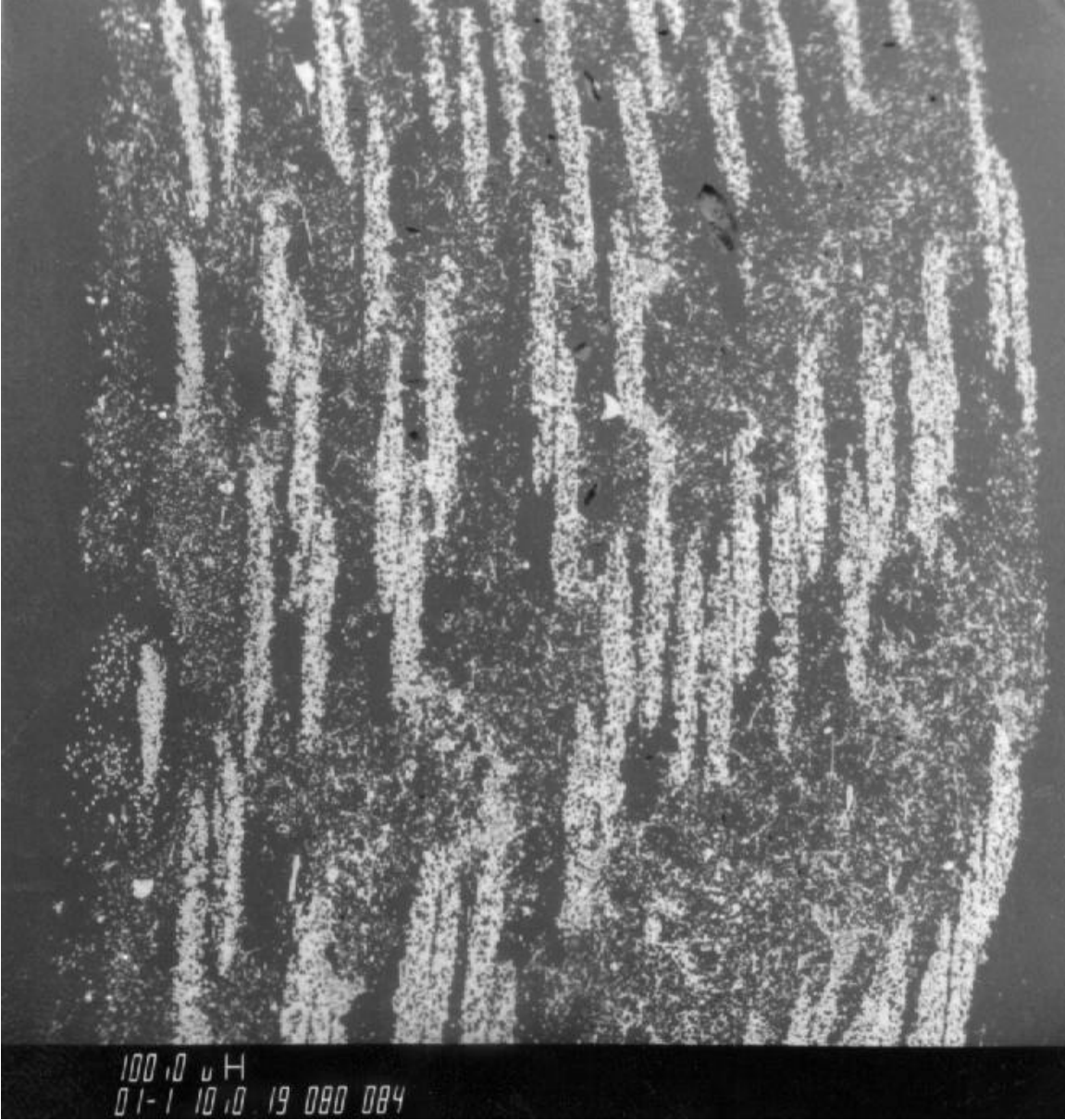
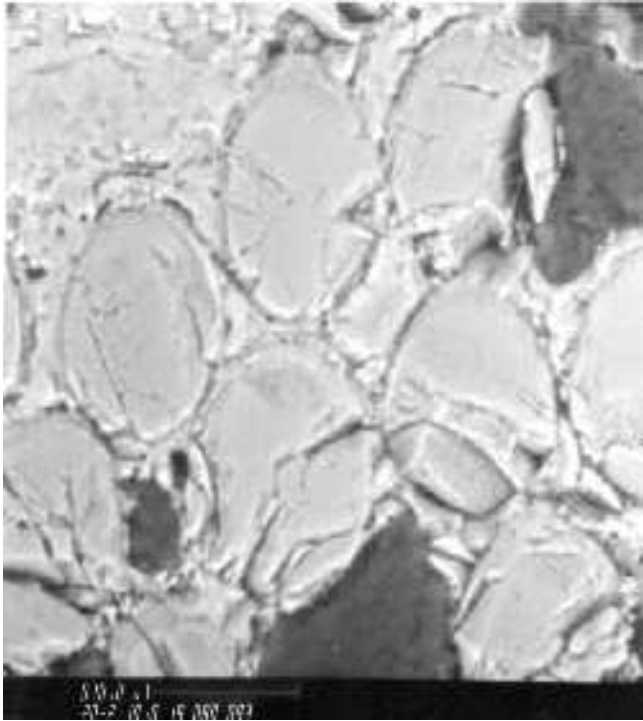
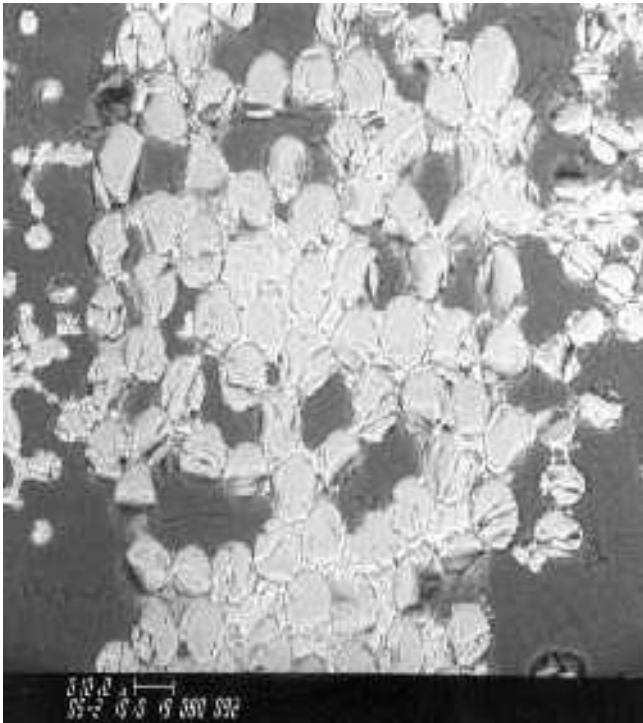


Figure 18. 20X BSE image of sample C3-2 from CFB thermal fatigue test.



**Figure 19. A. 500X BSE image of Nextel 610 fiber tow from sample C3-2 following CFB thermal fatigue test.**



**Figure 20. A. 500X BSE image of chopped fiber region of sample C3-2 following CFB thermal fatigue test. B. 2000X BSE image of chopped fiber and bond phase from sample C3-2.**

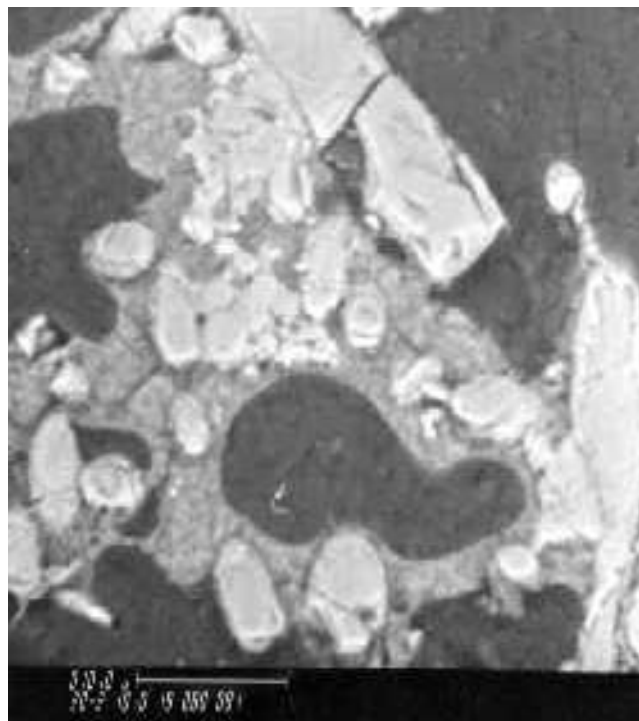
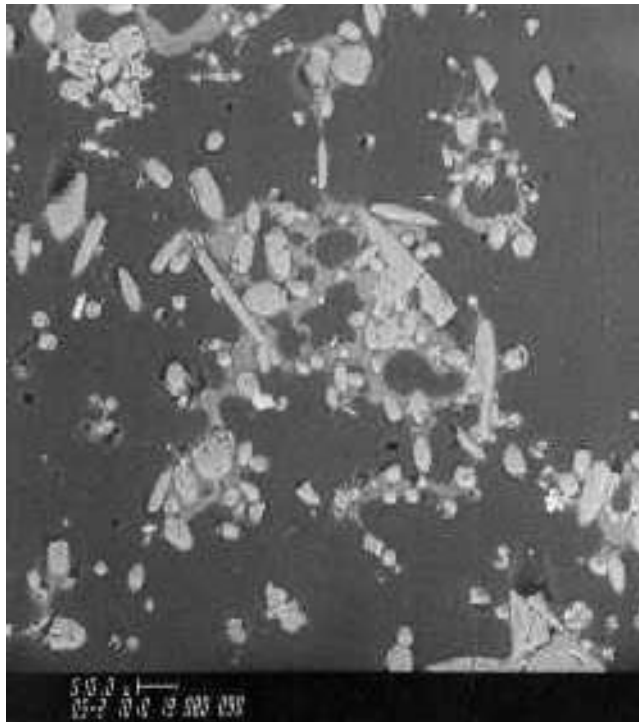
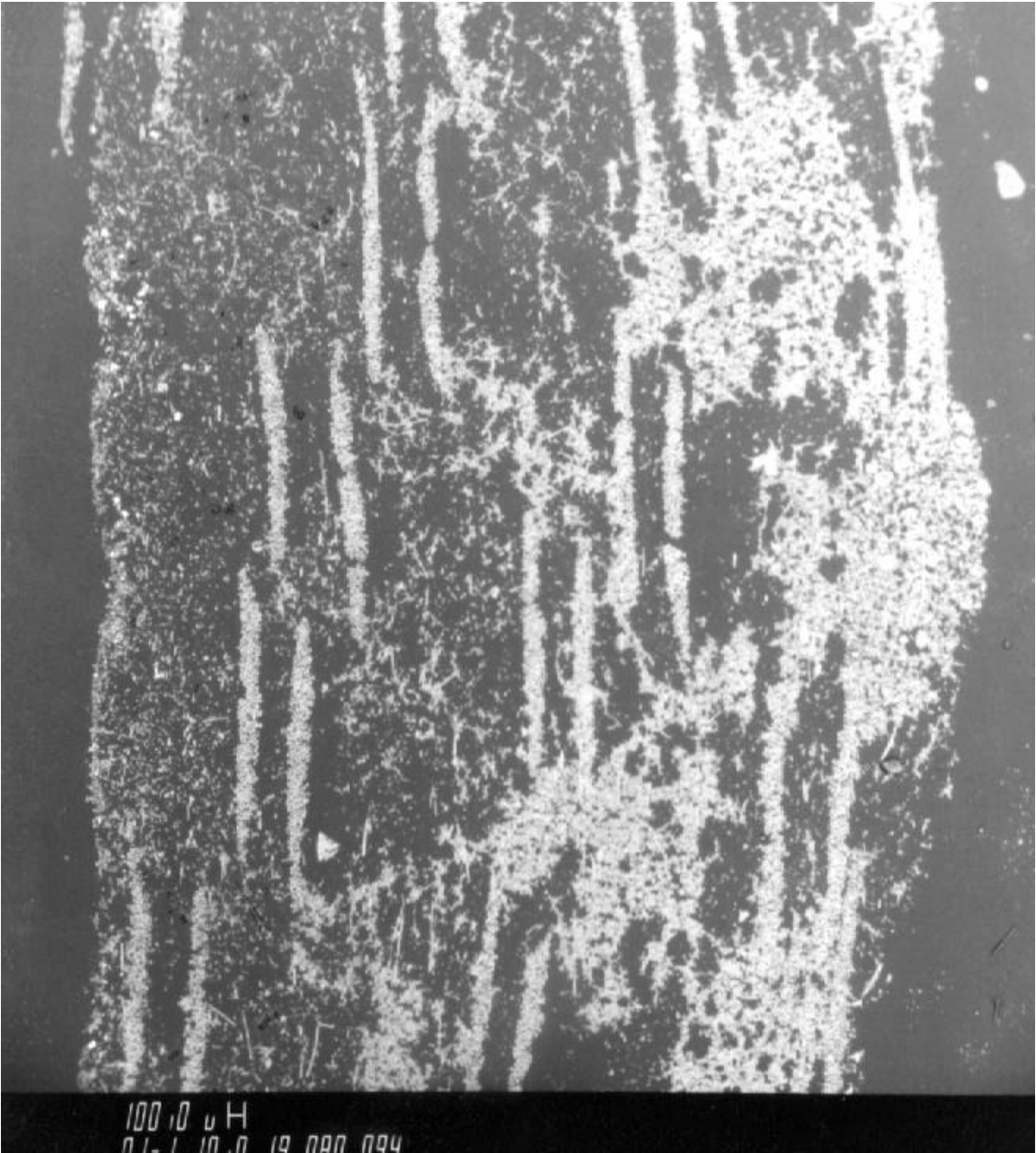
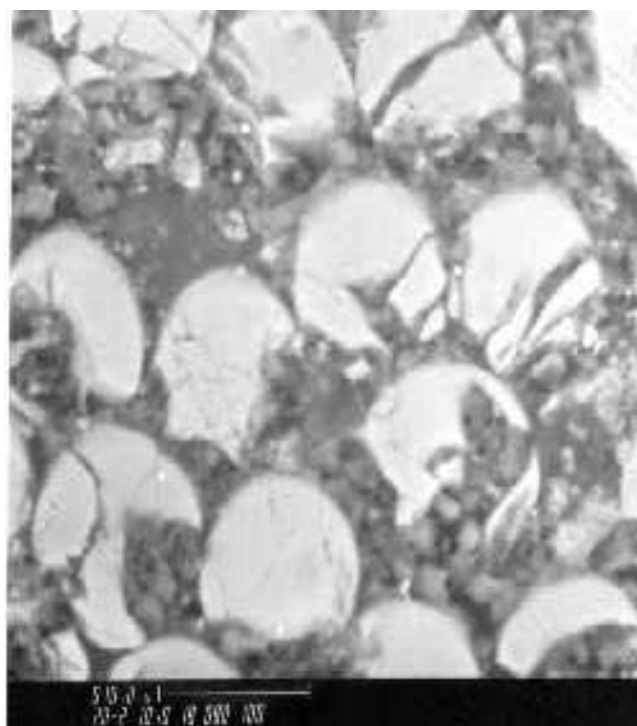
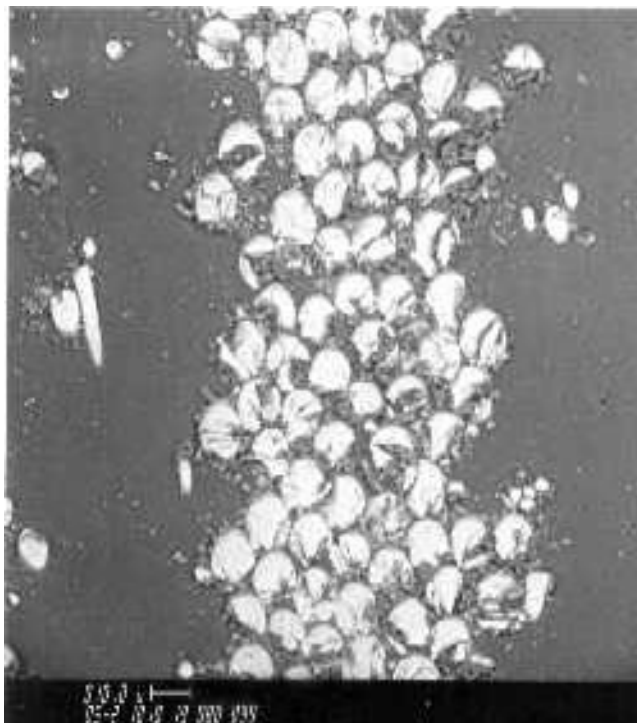


Figure 21. 20X BSE image of sample C4-4 from CFB thermal fatigue test.



**Figure 22. A. 500X BSE image of Nextel 610 fiber tow from sample C4-4. B. 2000X BSE image of individual Nextel 610 fibers in sample C4-4.**



**Figure 23. A. 500X BSE image of boehmite bonded chopped fibers in sample C4-4 from CFB thermal fatigue test. B. 2000X BSE image of boehmite bonded chopped fiber in sample C4-4.**

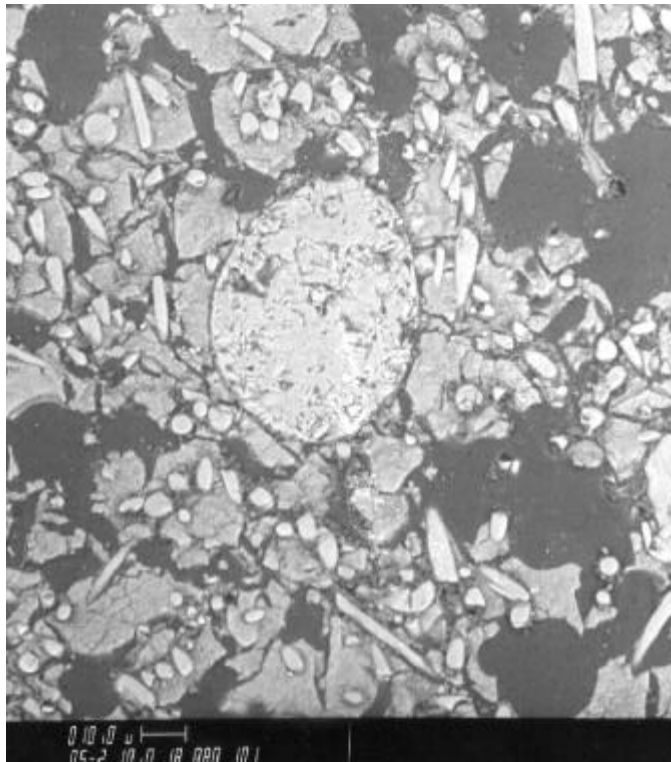


**Figure 24. Machined flange configuration.**



Figure 25. Flange test configuration and load-displacement results.

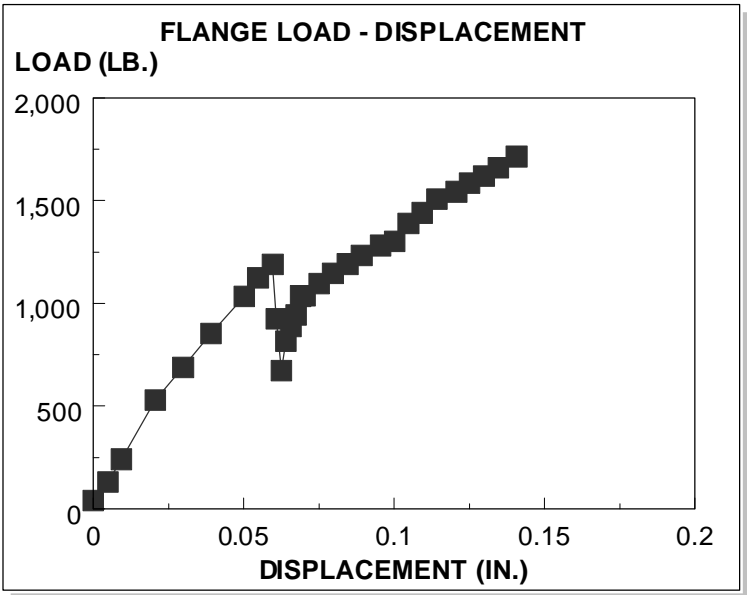
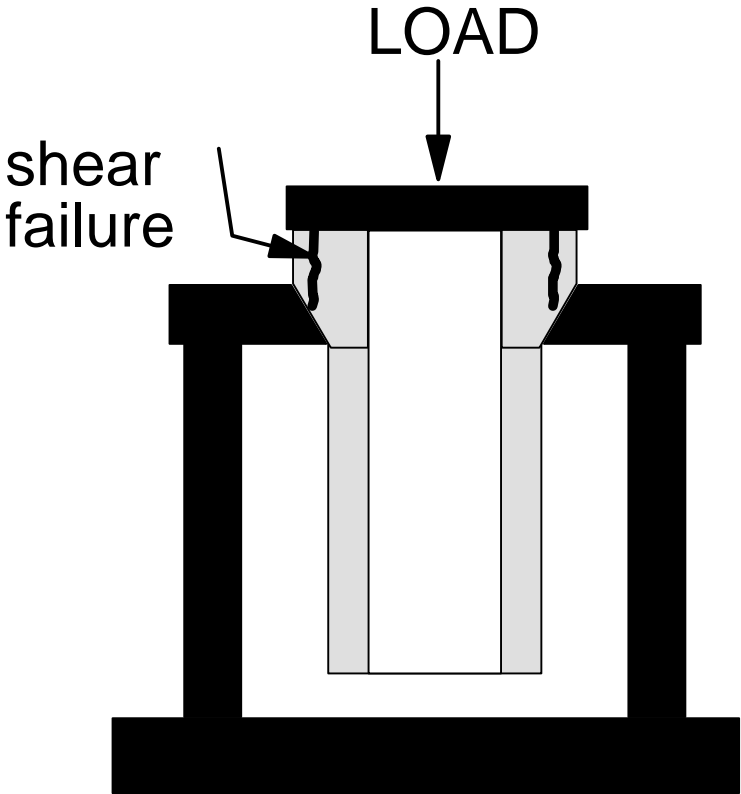


Figure 26. Composition and pressure drop results for W-STC HTHP 8/96 test.

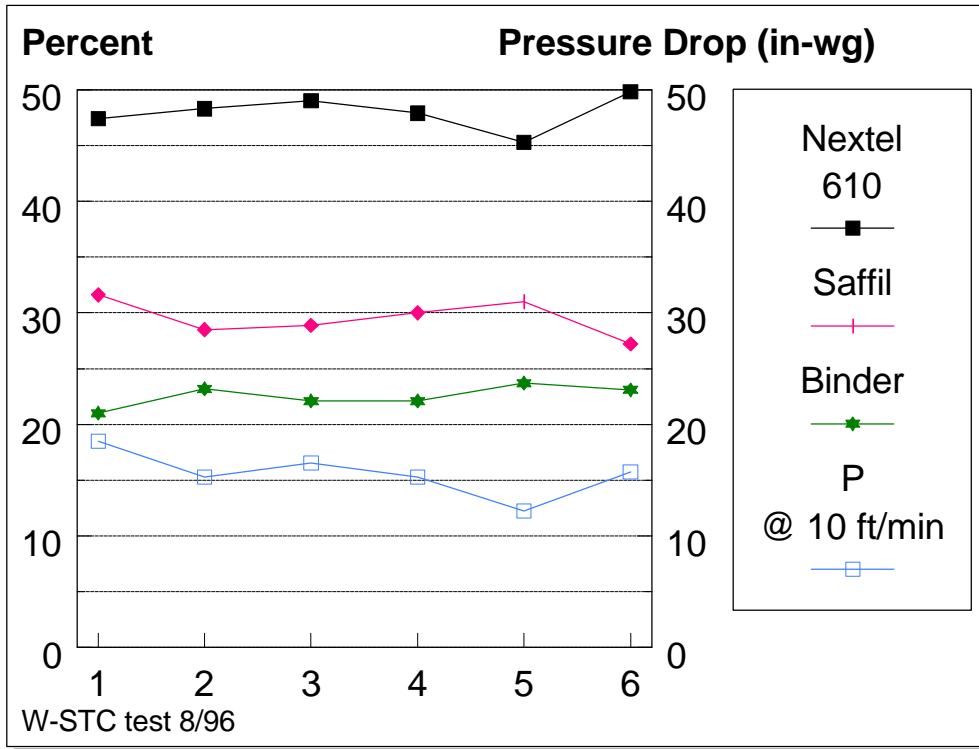


Figure 27. Compressive C-ring results for as-fabricated and post-test HTHP 8/96 test elements.

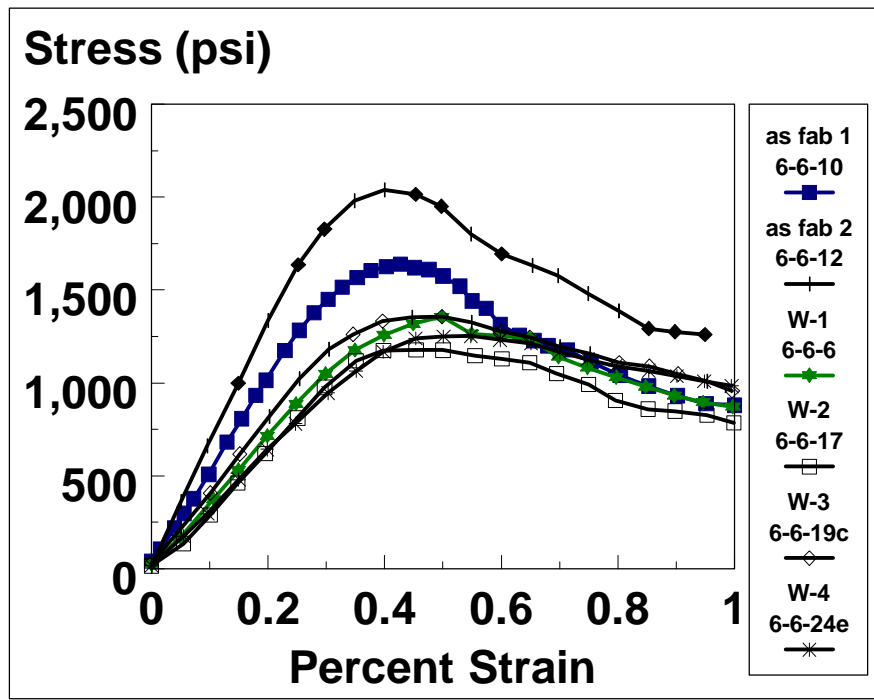


Figure 28. 20X BSE image of as-fabricated sample 6-6-10.

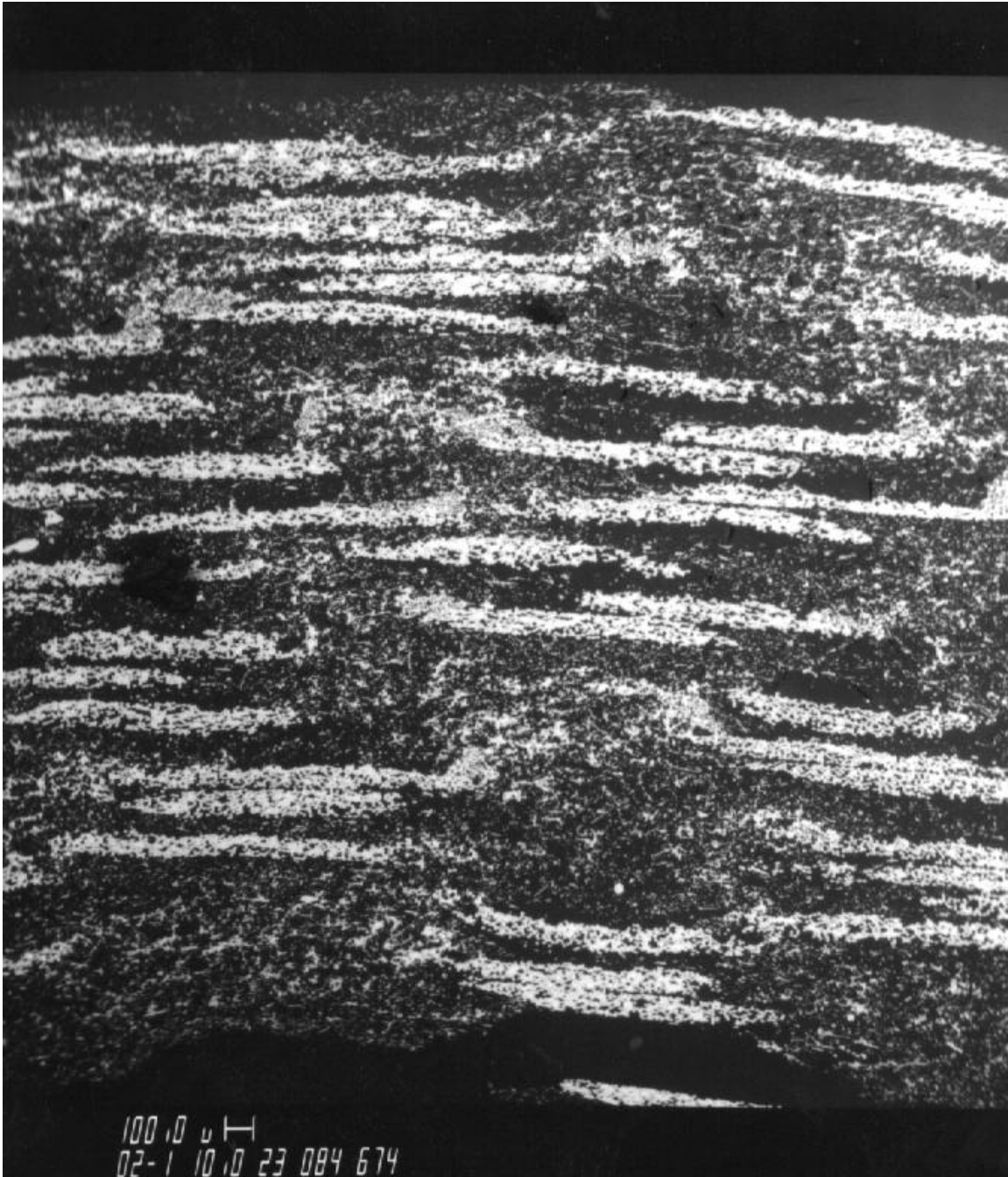
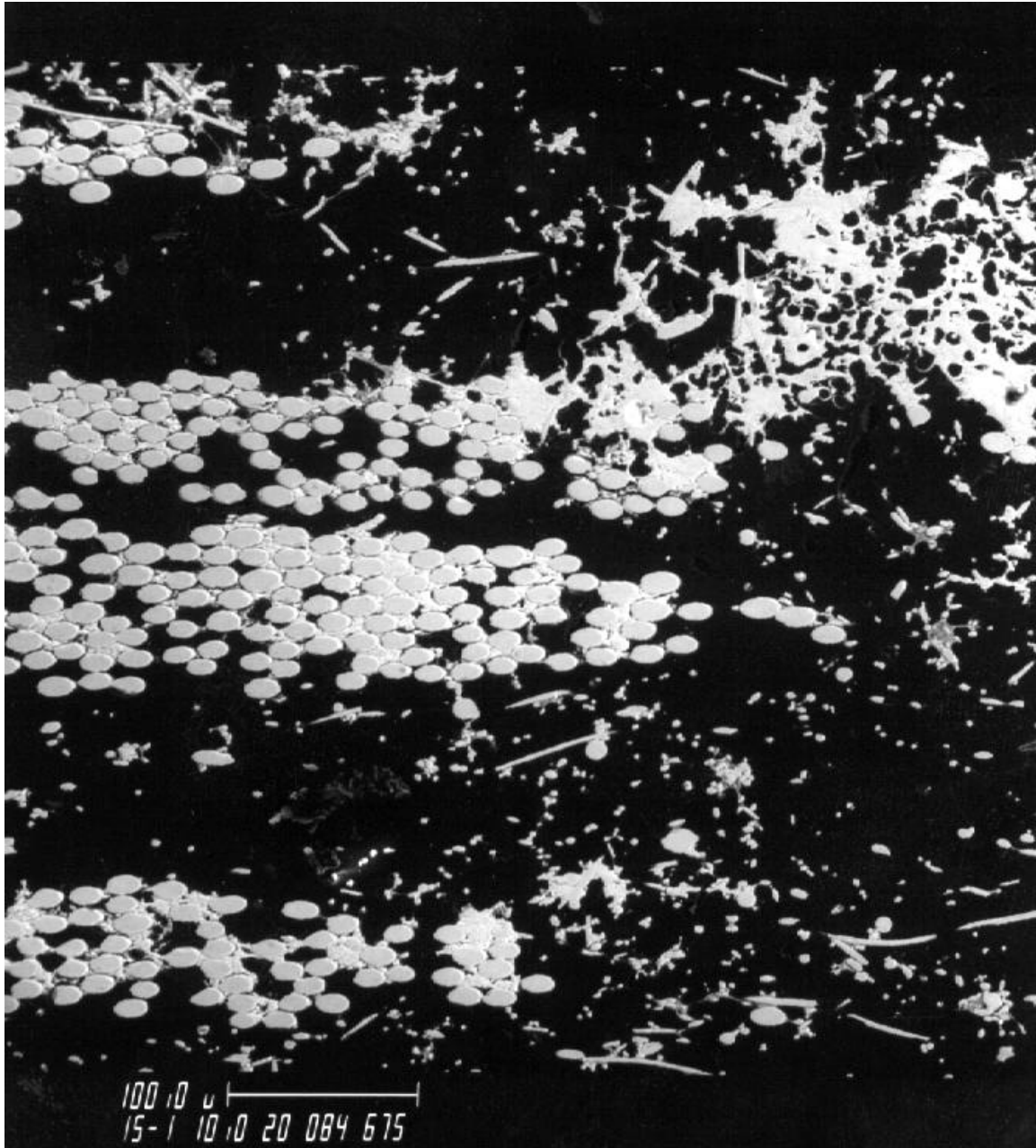
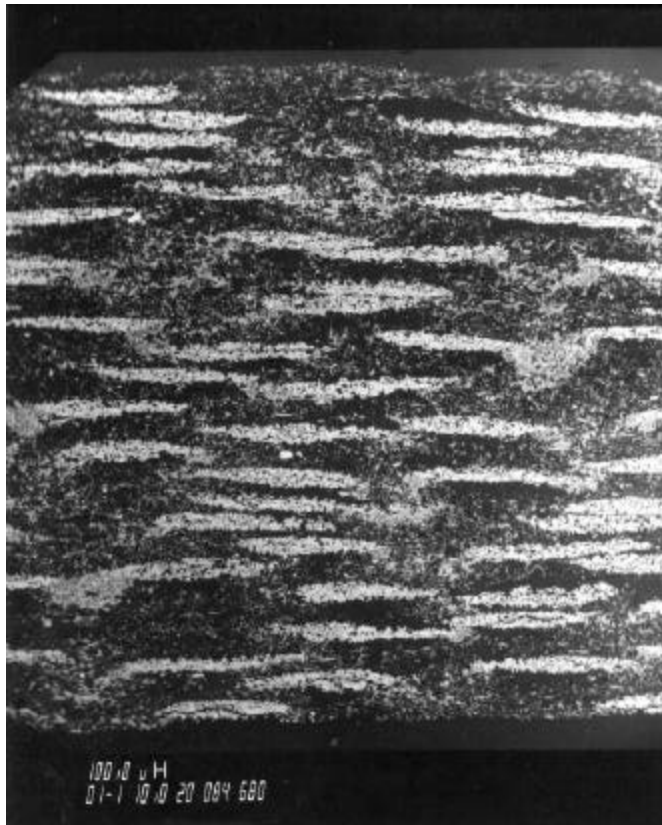


Figure 29. 150X BSE image of chopped fiber region in sample 6-6-10.



**Figure 30. 10X BSE image of sample 6-6-19 after W-STC HTHP test.**



**Figure 31. 150X BSE image of as-fabricated sample 6-6-19 after W-STC HTHP test.**

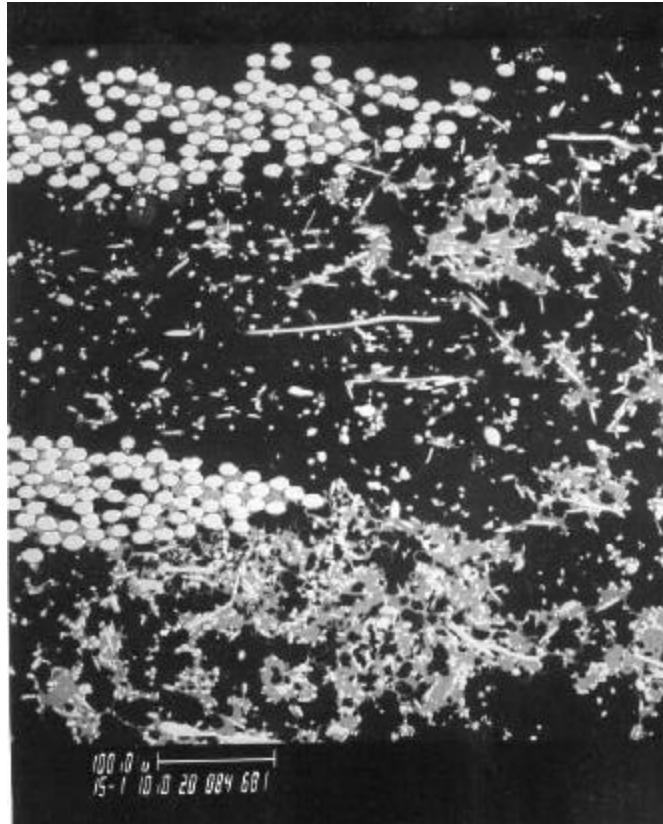


**Figure 32. 20X BSE image of the OD surface of sample 6-6-17 after W-STC HTHP test.**

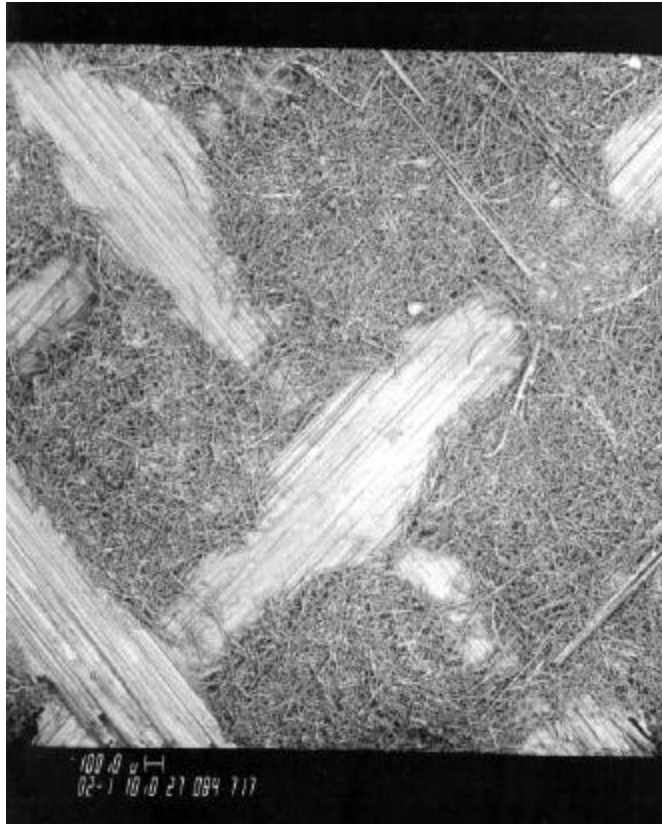


**Figure 33. 1000X BSE image of the OD surface of sample 6-6-17 after W-STC HTHP test.**

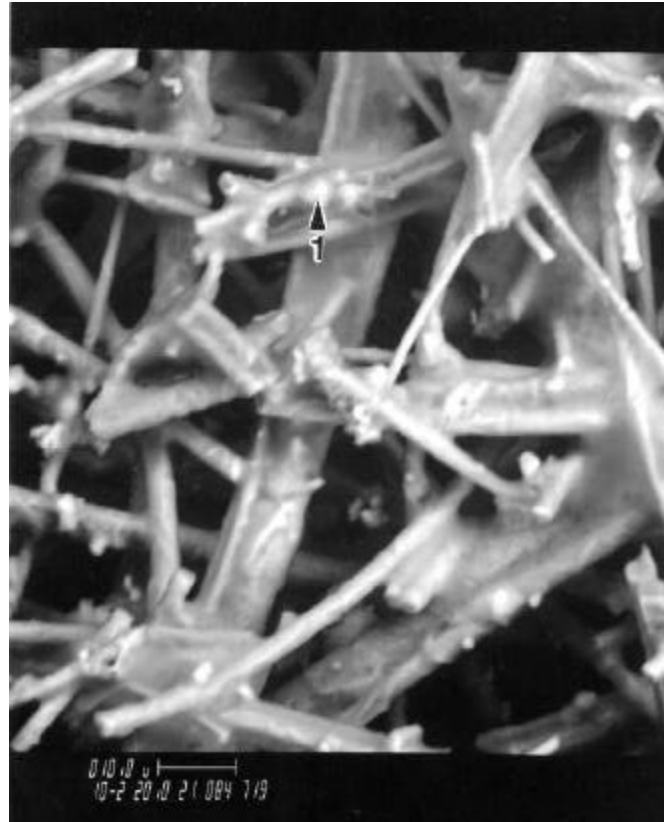


**Figure 34. 150X BSE image of sample 6-6-6 after W-STC HTHP test.**

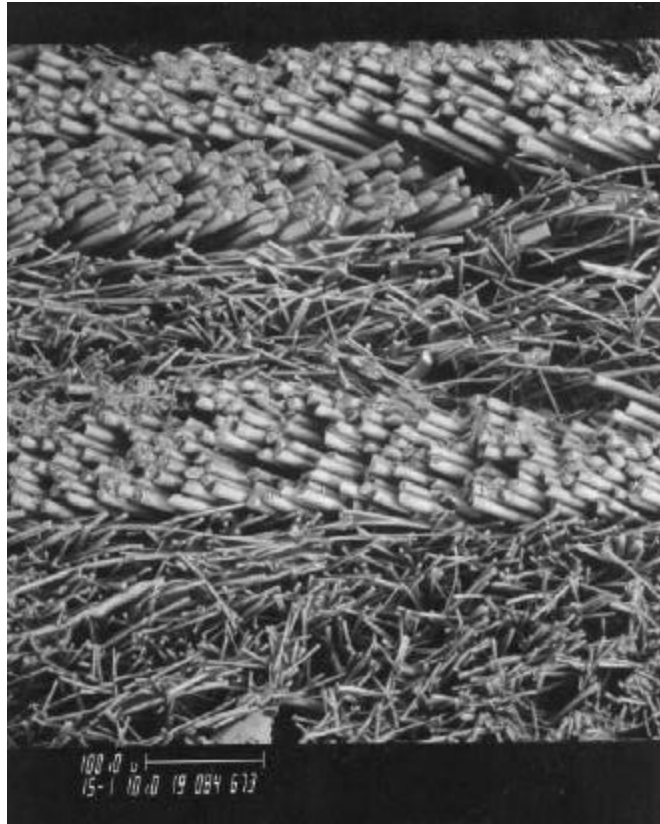


**Figure 35. 5X macrophoto of unserved Nextel 610 fiber.**



**Figure 36. 5X Macrophoto of rayon served Nextel 610 fiber.**

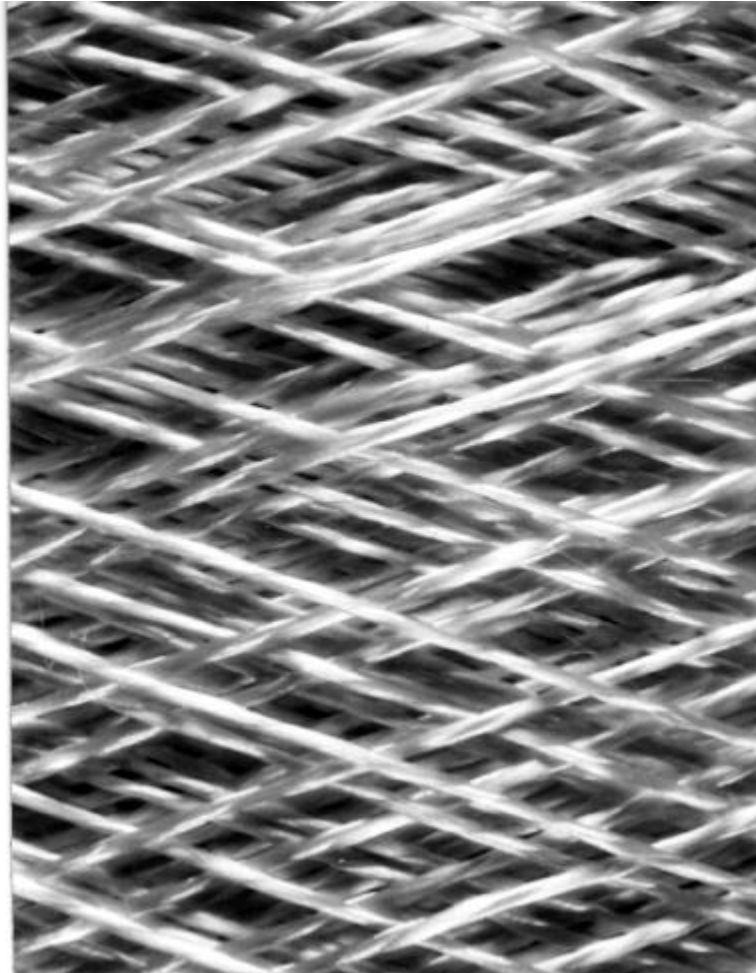


**Figure 37. Example of controlled fiber distribution.**

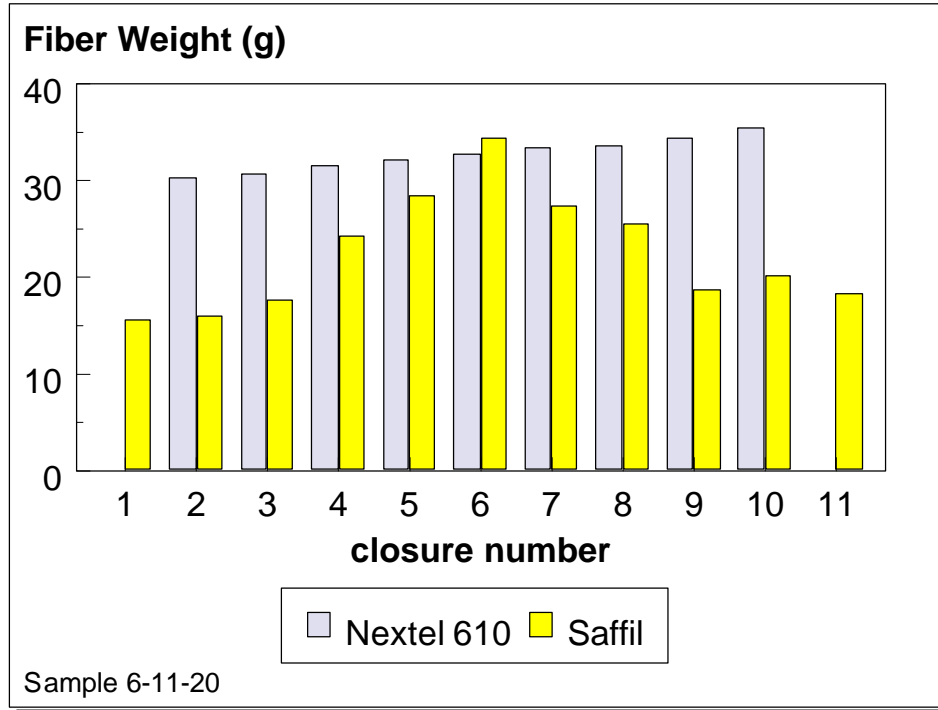


**Figure 38. Net shape flange configuration.**



**Figure 39. Compressive C-ring results for controlled fiber distribution with boehmite bond.**

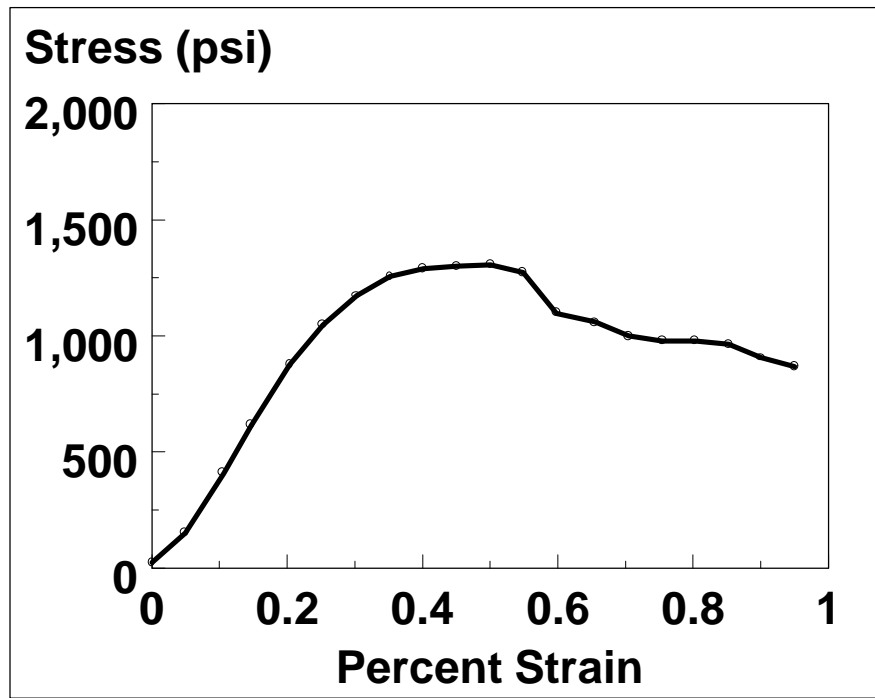
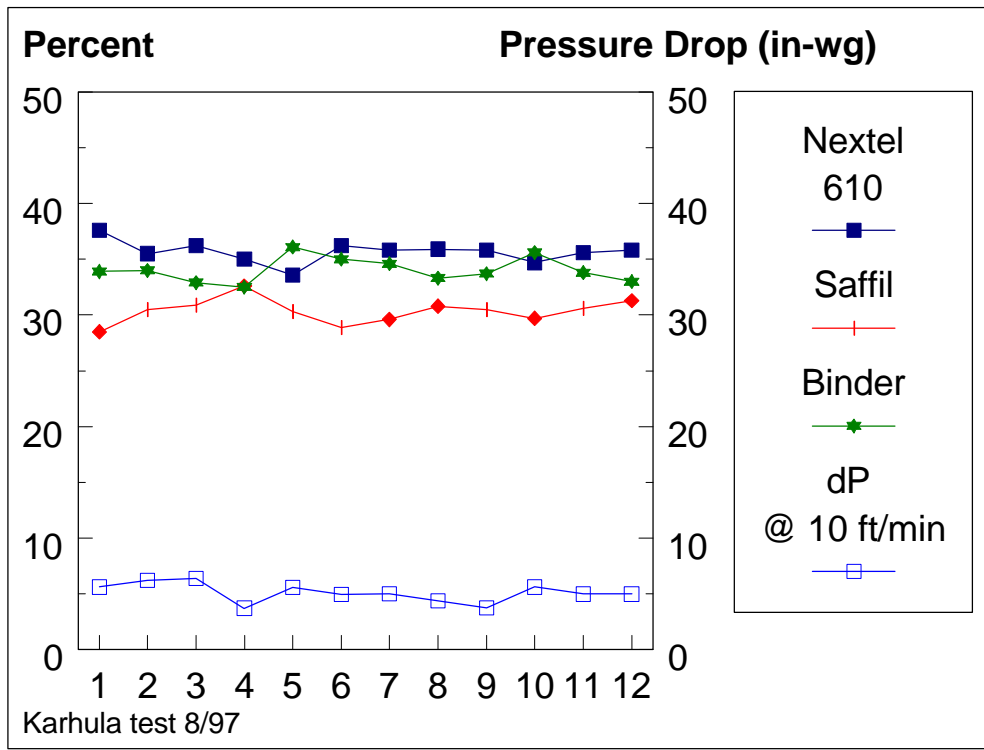


Figure 40. Filter element compositions and permeabilities for Karhula PCFB test.



**Figure 41. Surface defect on Karhula element.**



Figure 42. As-fabricated and post-test load-displacement results for Karhula elements.

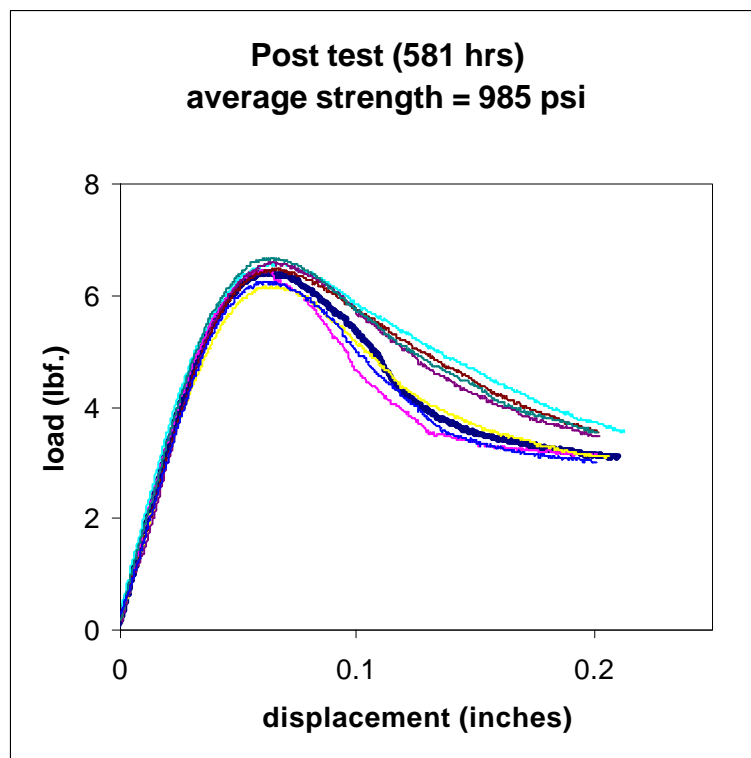
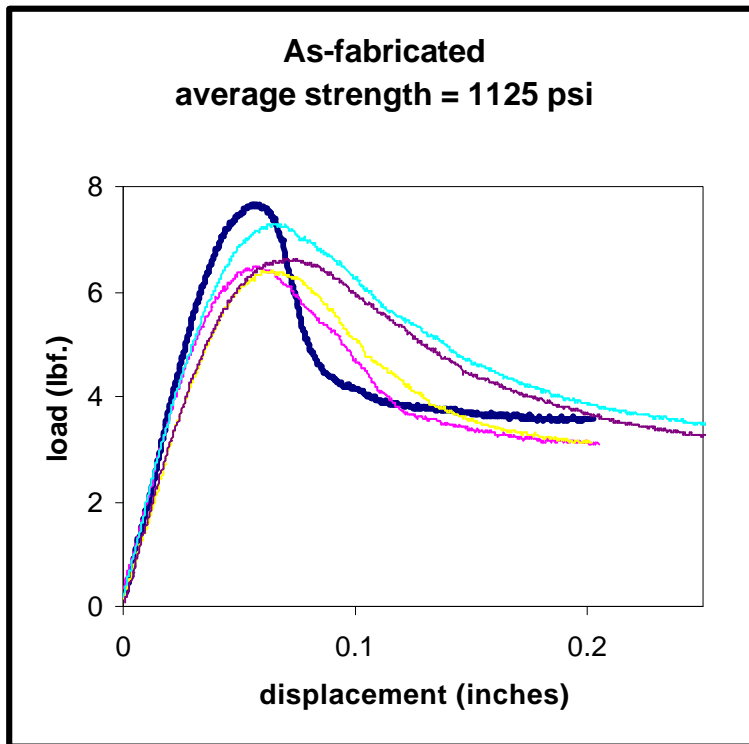
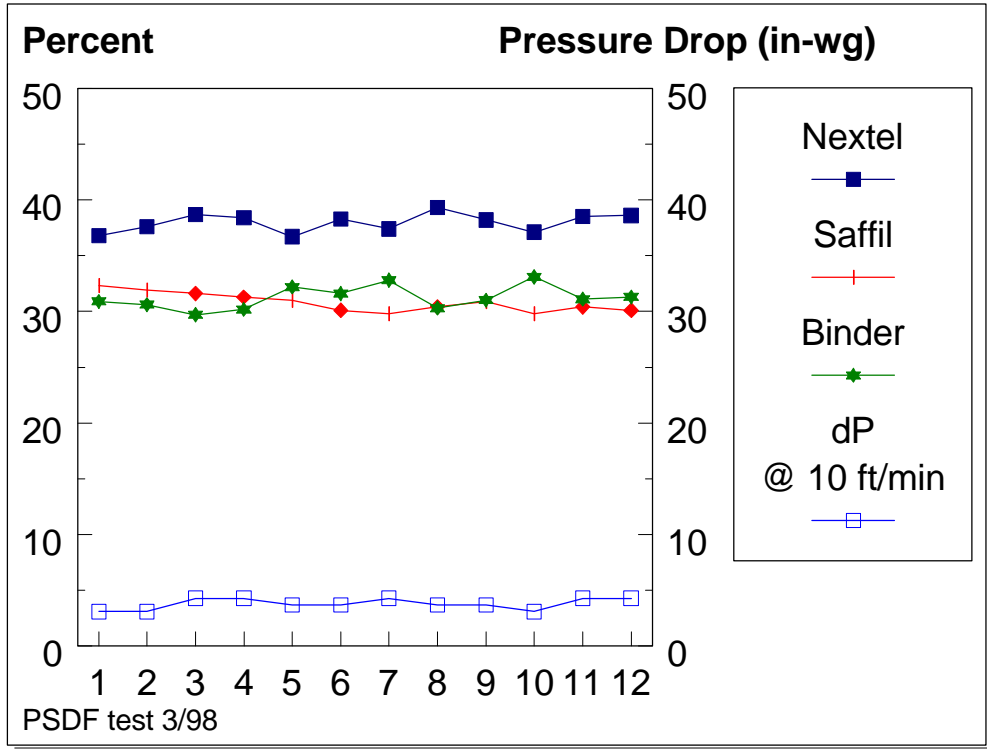
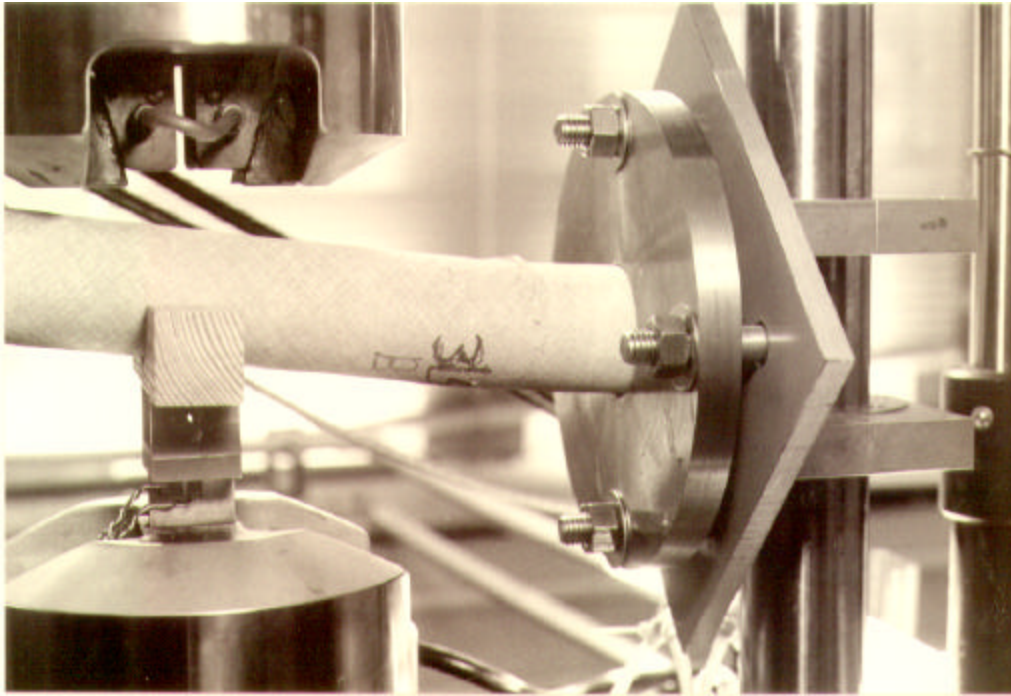
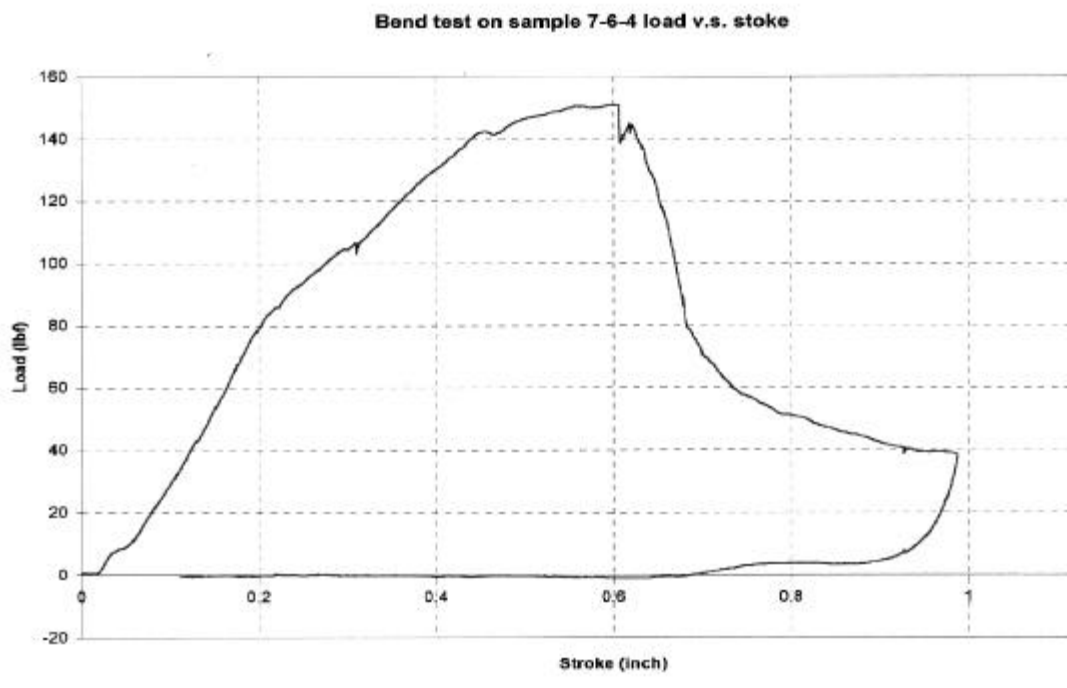


Figure 43. Composition and permeability of PSDF elements.





**Figure 44. Flange bend test configuration and load versus displacement results.**



## APPENDIX A: NEXTEL CERAMIC FIBER PROPERTIES

Property	Units	Nextel 610
Use Temperature	°C	1204
Filament Diameter	μm	10-12
Crystal Size	nm	<500
Crystal Type		Alpha alumina
Density	g/cm <sup>3</sup>	3.88
Filament Tensile Strength	MPa	2930
Filament Tensile Modulus	GPa	373
Surface Area	m <sup>2</sup> /g	<.2
Chemical Composition	wt%	>99 alumina
Thermal Expansion (100 - 1100 °C)	ppm/°C	7.9
Dielectric Constant	(@9.375 GHz)	~9.0
Refractive Index		1.735

## APPENDIX B: SAFFIL PROPERTIES

### Typical Physical Properties of SAFFIL Alumina Fiber

<b>melting point</b>	>2000	°C
<b>specific heat</b>	1	kJ/kg°C
<b>tensile strength</b>	$1.5 \times 10^3$	MN/m <sup>2</sup>
<b>Young's modulus</b>	$3 \times 10^5$	MN/m <sup>2</sup>
<b>median Diameter</b>	3.5	Microns
<b>shot content</b>	Negligible	
<b>alumina content</b>	95 - 97	%
<b>silica content</b>	3 - 5	%

### Property Changes during the Processing of Alumina Fiber

	<b>Eta</b>	<b>Eta Gamma</b>	<b>Gamma a</b>	<b>Gamma a Delta</b>	<b>Delta</b>	<b>Alpha Theta Mullite</b>	<b>Alpha Mullite</b>
<b>approx crystal size (Å)</b>	60				300 to 500	1000	2000+
<b>% crystallinity</b>	50	62	68	77	80-97	97	100
<b>% alpha alumina</b>					5-20	20-50	100
<b>pore volume mm<sup>3</sup>/g</b>	200		187	12	0 to 73	0	0
<b>shrinkage % at 1500°C (6 hrs)</b>	18	17	14	8	2-4	2	0
<b>typical tensile strength (MPa)</b>	2000			1800	1000 to 2000	1000	500

## Chemical Resistance of Saffil Alumina Fibers

Saffil has outstanding chemical stability and resistance to degradation in a variety of demanding conditions including reducing atmospheres and vacuums at high temperatures and when under attack from metal oxides. The high content of crystalline alumina in all grades of Saffil and the absence of free silica make Saffil stand out from the competition.

<b>Operating Atmospheres</b>	<b>Maximum Saffil Operation (°C)</b>
<b>Air</b>	<b>1600</b>
<b>Vacuum</b>	<b>1500</b>
<b>Hydrogen</b>	<b>1300</b>

## Transition Metal Oxides

In general terms transition metal oxides (eg Pb, Cu, Cr) act to reduce the melting point of fibres in the Al-Si system as these oxides vapourize at relatively low temperatures forming a eutectic blanket on the fibre surface. The rate of this reaction is considerably less for 96% alumina fibres such as Saffil due to the low levels of volatile silica giving Saffil longer lifetimes under these conditions than any other alumina containing fibre.

## Alkali Metals

Alkali metals (eg Na, Va) and their oxides also attack fibres in the Al-Si system. Saffil, however, is less susceptible to attack due to the high levels of alumina and low levels of silica. Our tests have shown that Saffil exposed to sodium vapour will form sodium aluminate and that lifetimes of furnace linings exposed to significant concentrations of alkali metal oxides can be in excess of six months.

## Acids

Saffil can be susceptible to attack from Fluoric Acid, Boric Acid, Phosphoric Acid and Hydrochloric Acid. However, in furnace applications these forms of attack will typically lead to premature failure of surrounding steelwork and supports before any serious damage occurs to the fibre.

## Low Alpha Grade

SAFFIL Low Alpha grades are high purity, polycrystalline alumina fibres available in bulk or milled form and engineered to be suitable for a range of high temperature insulation applications including module making, expansion joints, furnace repairs, vacuum formed boards, custom shapes and papers.

## Properties

Manufactured by a unique solution extrusion process to ensure the highest levels of chemical purity, the lowest possible levels of shot content (non-fibrous particles) and exceptional control of fibre diameter, SAFFIL Low Alpha grades are manufactured to be resistant to thermal shrinkage and chemical attack up to 1600°C.

All SAFFIL Low Alpha products are manufactured with a chemical composition of 96% alumina and 4% silica with impurities typically totalling less than 0.5%. The fibre diameter is very tightly controlled with a median of around 3 microns, with virtually no fibres of less than 1 micron in diameter.

## Uses and Benefits

AFFIL Low Alpha bulk grade when used as a main component of modules, boards and papers provides cost effective levels of thermal stability unmatched by

other commercially available insulating fibres. Low thermal shrinkage translates directly into long life and reduced fuel and maintenance costs, while low thermal conductivity gives superior insulation properties to products containing SAFFIL Low Alpha products.

Blended products manufactured using SAFFIL, alumino-silicate fibres and proprietary binder systems give exceptional, cost effective performance up to 1600°C. In these mixed fibre systems, low alpha grade SAFFIL provides an alumina matrix within which the lower performance alumino-silicate fibres are stabilised.

At elevated temperatures silica migration from the alumino-silicate fibres occurs leading to the formation of a highly stable mullite phase. This reaction provides an extremely favourable increase in the thermal dimensional stability of the alumino-silicate board. Mixed fibre systems of this type can be engineered to show specific shrinkages at their application temperatures through the addition of specific levels of SAFFIL Low Alpha fibre.

## Chemical Stability

SAFFIL Low Alpha products have proven themselves highly resistant to chemical attack which occurs in insulating fibres when metal oxides attack volatile silica molecules at high temperatures. As SAFFIL contains silica in only a small percentage as a crystalline growth inhibitor and as it does not include any free silica it is less susceptible to chemical attack than insulating fibres with a high silica content.

## APPENDIX C: NYACOL COLLOIDAL ALUMINA PROPERTIES

### Nyacol® Colloidal Alumina

Nyacol AL20 is designed specifically for use in high-temperature vacuum-formed fibrous refractories. It provides a good balance of particle size, concentration and pH to enhance the binding characteristics while optimizing the economics of a binder system. Nyacol AL20 is effective in high-temperature refractories as a stable binder where colloidal silica binders fail. Its other uses are as a catalyst support/binder and as a ceramic binder.

Typical Properties		
	AL20	AL20DW
Wt.% Al <sub>2</sub> O <sub>3</sub>	20	20
Particle size, nm	50	50
Particle charge	positive	positive
pH	4.0	4.0
Specific gravity	1.19	1.19
Viscosity, cps	10	10

Nyacol AL20SD is an alumina powder that is dispersible in either water or ethylene glycol. Its dispersibility in other polar solvents is subject to testing. It can be used in applications where a water based system cannot be used.

Typical Properties	
	AL20SD
Form	White powder
Wt.% Al <sub>2</sub> O <sub>3</sub> *	78
Particle size, nm	50 (when dispersed)
Particle charge	positive
% Free water	4.0

## References

---

- <sup>1</sup> R. S. Hay, "Sol-Gel Coating of Fiber Tows", *Ceram. Eng. Sci. Proc.* 12[7-8] pp. 1064-1074 (1991).
- <sup>2</sup> Kingery, W. D., "Fundamental Study of Phosphate Bonding in Refractories: I, Literature Review", *Acers. Journal* 33[8] ; 239-241 (1950).
- <sup>3</sup> Chiou, J and D. D. L. Chung, "Improvement of the temperature resistance of aluminum-matrix composites using an acid phosphate binder", *J. Mat'ls Sci* 28 p 1435-1446 (1993).
- <sup>4</sup> R. C. MacKenzie, Differential Thermal Analysis, Academic Press, p. 280-281, (1970).
- <sup>5</sup> Leiser, D. B., et. al., "Developments in Fibrous Refractory Composite Insulation", *Acers. Bull.*, (60) 11, p1201-1204, (1981).
- <sup>6</sup> Creedon, J. F., et. al., "Strength and Thermal Stability Improvement of Fibrous Ceramic Composites", *Sampe Quarterly*, p 9-15, October 1983.
- <sup>7</sup> Li, H., "Fracture of Aluminum Phosphate/Alumina Matrix Silicon Carbide Fiber Reinforced Laminated Composites", Ph.D. Thesis, Univ. of Nevada, Reno 1992
- <sup>8</sup> Huang, X and K. L. Reifsnider, "A Ligature Model for Fiber Reinforced Porous Composites", submitted for publication in *Advanced Composites Letters*.